

Investigating Lorentz Invariance Violation with the long baseline experiment P2O

Nishat Fiza^{a,1} Nafis Rezwan Khan Chowdhury^{b,c,2} Mehedi Masud^{d,3}

^a*Department of Physical Sciences, IISER Mohali, Knowledge City, SAS Nagar, Mohali - 140306, Punjab, India*

^b*Institut de Física Corpuscular (CSIC-Universitat de València), Parc Científic de la UV C/ Catedrático José Beltrán, 2, E-46980 Paterna (València), Spain*

^c*Department of Physics and Astronomy, University of Utah 115 S. 1400 E., Salt Lake City, Utah 84112*

^d*Center for Theoretical Physics of the Universe, Institute for Basic Science (IBS), Daejeon 34126, Korea*

E-mail: ph15039@iisermohali.ac.in, nafis.chowdhury@ific.uv.es, masud@ibs.re.kr

ABSTRACT: One of the basic propositions of quantum field theory is Lorentz invariance. The spontaneous breaking of Lorentz symmetry at a high energy scale can be studied at low energy extensions like the Standard model in a model-independent way through effective field theory (EFT). The present and future Long-baseline neutrino experiments can give a scope to observe such a Planck-suppressed physics of Lorentz invariance violation (LIV). A proposed long baseline experiment, Protvino to ORCA (dubbed "P2O") with a baseline of 2595 km, is expected to provide good sensitivities to unresolved issues, especially neutrino mass ordering. P2O can offer good statistics even with a moderate beam power and runtime, owing to the very large (~ 6 Mt) detector volume at KM3NeT/ ORCA. Here we discuss in detail, how the individual LIV parameters affect neutrino oscillations at P2O and DUNE baselines at the level of probability and derive analytical expressions to understand interesting degeneracies and other features. We estimate $\Delta\chi^2$ sensitivities to the LIV parameters, analyzing their correlations among each other, and also with the standard oscillation parameters. We calculate these results for P2O alone and also carry out a combined analysis of P2O with DUNE. We point out crucial features in the sensitivity contours and explain them qualitatively with the help of the relevant probability expressions derived here. Finally we estimate constraints on the individual LIV parameters at 95% confidence level (C.L.) intervals stemming from the combined analysis of P2O and DUNE datasets, and highlight the improvement over the existing constraints. We also find out that the additional degeneracy induced by the LIV parameter a_{ee} around -22×10^{-23} GeV is lifted by the combined analysis at 95% C.L.

Contents

1	Introduction	1
2	Theoretical background	3
3	Impact of LIV parameters on probability	5
4	Simulation details	11
5	Correlations among the LIV parameters	14
6	Degeneracies with the standard oscillation parameters	18
7	Bounds on the LIV parameters	20
8	Summary and conclusion	22

Contents

1 Introduction

The phenomenon of neutrino oscillation which was first experimentally established more than twenty years back from the observations of atmospheric and solar neutrinos [1, 2] is one of the most transparent currently available portals into the rich physics beyond the standard model (BSM) of particle physics. In standard scenario neutrino oscillation is governed by six parameters, namely the three mixing angles ($\theta_{12}, \theta_{13}, \theta_{23}$); one Dirac CP phase (δ_{13}), and two mass-squared differences ($\Delta m_{21}^2, \Delta m_{31}^2$). So far $\theta_{12}, \theta_{13}, \Delta m_{21}^2$ and the magnitude $|\Delta m_{31}^2|$ have been measured with good precision from various neutrino experiments. One of the principal focus of the neutrino oscillation community is now on the measurement and implications of the values of the remaining parameters: the leptonic (Dirac) CP phase δ_{13} , the sign of Δm_{31}^2 (denoting the correct neutrino mass ordering) and the octant of the mixing angle θ_{23} . A value of δ_{13} not equal to zero or π would indicate CP violation in the lepton sector. This, in turn, can potentially shed light on the another fundamental puzzle, namely the baryon asymmetry of the universe [3]. Resolution of the correct mass ordering and octant can help narrow down the plausible set of models explaining neutrino mass generation.

Presently running long-baseline neutrino oscillation experiments Tokai to Kamioka (T2K) [4] and NuMI Off-axis ν_e Appearance (NO ν A) [5] are already giving us glimpses to the resolutions of the issues mentioned above. T2K data [6] has ruled out CP conservation ($\delta_{13} \simeq 0, \pi$) at 95% confidence limit (C.L.). Irrespective of the mass ordering, at 99.73%

C.L. (3σ) T2K excludes 42% of the entire parameter space for δ_{13} (mostly around $+\pi/2$), restricting the allowed region to roughly $\delta_{13} \in [-\pi, 0.04\pi] \cup [0.89\pi, \pi]$. $\text{NO}\nu\text{A}$ data [7], on the other hand indicates a slight preference for θ_{23} lying in the higher octant (HO) at a C.L. of 1.6σ . It also excludes most of the choices near $\delta_{13} = \pi/2$ at a C.L. $\geq 3\sigma$ for inverted mass ordering (IO). These measurements are expected to become more accurate as more data pour in. Though the global analyses of neutrino data [8–11] shows an indication towards NO with θ_{23} possibly lying in the higher octant, the CP phase still has a large uncertainty.

In near future, various other next-generation neutrino experiments with more sophisticated detection technologies are expected to start taking data. These experiments include, among others, Deep Underground Neutrino Experiment (DUNE) [12, 13], Tokai to Hyper-Kamiokande (T2HK) [14], Tokai to Hyper-Kamiokande with a second detector in Korea (T2HKK) [15], European Spallation Source ν Super Beam (ESS ν SB) [16], Jiangmen Underground Neutrino Observatory (JUNO) [17], Protvino to ORCA (P2O) [18]. These experiments are expected to reach upto an unprecedented (\sim a few percent) level of precision in measuring the oscillation parameters and hence are also susceptible to the presence of various possible new physics.

CPT symmetry, one of the most sacred foundations in local relativistic quantum field theory, is based on the assumptions of the hermiticity of the hamiltonian, Lorentz invariance and local commutativity. Since an interacting theory with CPT violation also breaks Lorentz invariance [19], one widely used strategy to probe CPT violation is to analyze the associated Lorentz invariance violation (LIV). Spontaneous breakdown of Lorentz invariance may occur in theories of quantum gravity (in string theory, for *e.g.*) at Planck scale ($M_P \sim 10^{19}$ GeV), forcing a Lorentz tensor field to acquire a non-zero vacuum expectation value, thus selecting a preferred spacetime direction [20–24]. It has been shown in literature that the Standard Model (SM) of particle physics can be extended to construct a low energy effective field theory (EFT), namely Standard Model Extension (SME) [25–27] that includes such Lorentz invariance violating effects, suppressed by M_P . Neutrino oscillation by virtue of its interferometric nature, can probe such LIV effects at SME, thereby offering us a probe to the Planck scale physics.

A broad range of experimental parameters such as neutrino-beam flavor composition, length, direction, and energy, as well as detector techniques provide different and often complementary sensitivities to the many higher dimensional operators characterizing LIV at accessible range of energies. Indeed, constraints on LIV parameters of SME have been obtained analysing the data from several neutrino experiments, - LSND [28], MINOS [29, 30], MiniBooNE [31], Double Chooz [32], Super-Kamiokande [33], T2K [34], IceCube [35]. Outside the experimental collaboration also, there exist studies to explore LIV and CPT-violation, - for *e.g.*, in long-baseline accelerator neutrinos [36–44], short-baseline reactor antineutrinos [45], atmospheric neutrinos [46–49], solar neutrinos [50], and high-energy astrophysical neutrinos [51–53]. Recently, the authors of [54] have explored higher dimensional LIV parameters in the context of muon $g-2$ measurements by analysing available oscillation data for $\text{NO}\nu\text{A}$ and T2K. For a comprehensive list of constraints on all the LIV parameters collected together we refer the readers to reference [55].

The proposed P2O experiment [18, 56–58] will have a baseline extending approximately

2595 km from the Protvino accelerator complex to the ORCA/KM3NET detector at the Mediterranean, - both of which are already existing. P2O baseline is most sensitive to first $\nu_\mu \rightarrow \nu_e$ oscillation maxima around 4-5 GeV. Neutrino interaction around this energy is dominated by Deep Inelastic Scattering which is relatively well described theoretically, compared to, for *e.g.*, 2-2.5 GeV (for DUNE) where resonant interactions and nuclear effects can potentially impact the measurements more significantly [59–64]. Such a very long baseline and relatively higher energy of the oscillation maxima gives P2O an excellent level of sensitivity, especially towards neutrino mass ordering. As has been illustrated in reference [65], the P2O baseline is favourable to determine mass hierarchy also due to the much less interference by the hierarchy-CP phase degeneracy. The very large detector volume of 6 Mt at ORCA will allow to detect thousands of neutrino events per year even with a very large baseline and a moderate beam power, - subsequently offering sensitivities to neutrino mass ordering, CP violation and θ_{23} -octant that are competitive with the current and upcoming long-baseline neutrino experiments¹ [18, 66]. Recently it has been proposed that it is also possible to reach unprecedented sensitivity to leptonic CP violation at P2O using tagged neutrino beams by utilizing the kinematics of neutrino production in accelerators and recent advances in silicon particle detector technology [67]. In recent years, there has been some interests in estimating new physics capabilities of P2O. Reference [68] discussed the sensitivity reach of P2O to Non-unitarity of the leptonic mixing matrix and also estimated how it will affect the standard physics searches. The authors of [65] discussed about the possible optimization of P2O in order to explore non-standard neutrino interactions. In the present work, we analyze the capabilities of P2O to probe violations of Lorentz invariance and CPT symmetry to estimate the constraints that can be put on these new physics parameters.

The present manuscript is organised as follows. In Sec. 2 we briefly describe the formalism of LIV. In Sec. 3 we discuss in detail the probability expressions in presence of LIV parameters and provide a thorough analysis of the changes induced by each LIV parameter by means of heatplots. Sec. 4 describes the simulation procedures followed in this work. Secs. 5 and 6 illustrate the $\Delta\chi^2$ sensitivity results showing the correlations of LIV parameters among themselves and with the standard oscillation parameters δ_{13} and θ_{23} . Sec. 7 shows our final results as the constraints on LIV parameters obtained from this work, followed by the summary and conclusion in Sec. 8.

2 Theoretical background

We follow the widely used formalism of introducing Planck-suppressed CPT/Lorentz invariance violating effect to write a Lagrangian for the Standard Model Extension (SME), as developed in [25–27, 69–72]. The Lagrangian relevant for neutrino propagation in SME is then given by,

$$\mathcal{L} = \frac{1}{2} \bar{\Psi}(i\not{\partial} - M + \hat{\mathcal{Q}})\Psi + h.c., \quad (2.1)$$

¹P2O in its nominal configuration with a 90 kW beam, can resolve mass ordering with $\gtrsim 6\sigma$ sensitivity in 5 years of running, and also has a projected sensitivity of more than 3σ to θ_{23} -octant with 3 years of running. With a 450 kW beam, it can offer 2σ sensitivity to δ_{13} after 3 years of operation.

where Ψ is the spinor containing the neutrino fields. The first two terms inside the parentheses are the usual kinetic and the mass terms in the SM Lagrangian while the LIV effect has been incorporated by the operator \hat{Q} . The Lorentz invariance violating term, which is suppressed by Planck-mass scale M_P can be written in terms of the basis of the usual gamma-matrix algebra. Considering only renormalizable and only the CPT-violating LIV terms, one can write the LIV Lagrangian from Eq. 2.1 in terms of vector and pseudovectors [25],

$$\mathcal{L}_{\text{LIV}} \supset -\frac{1}{2} \left[a_{\alpha\beta}^\mu \bar{\psi}_\alpha \gamma_\mu \psi_\beta + b_{\alpha\beta}^\mu \bar{\psi}_\alpha \gamma_5 \gamma_\mu \psi_\beta \right], \quad (2.2)$$

where a_μ, b_μ are constant hermitian matrices and are in general combinations of tensor expectations, mass parameter and coefficients arising from the decomposition of gamma matrices. We focus on the following CPT-violating LIV parameter that is relevant in the context of the propagation of left handed neutrinos,

$$(a_L)_{\alpha\beta}^\mu = (a + b)_{\alpha\beta}^\mu. \quad (2.3)$$

Since our focus is on the isotropic component of the LIV terms, we will make the Lorentz indices zero. To further simplify our notation we will henceforth denote the parameter $(a_L)_{\alpha\beta}^0$ as $a_{\alpha\beta}$ ².

Using spinor redefinitions to get rid of the non-trivial time derivatives in the Lorentz invariance violating Lagrangian in Eq. 2.1 and carrying out some lengthy algebra with the resulting modified Dirac equation one can derive the Lorentz invariance violating effective hamiltonian relevant for ultrarelativistic, left-handed neutrino propagation through matter [71, 72, 74].

$$\begin{aligned} H &\simeq \underbrace{\frac{1}{2E} U \begin{pmatrix} m_1^2 & 0 & 0 \\ 0 & m_2^2 & 0 \\ 0 & 0 & m_3^2 \end{pmatrix} U^\dagger}_{H_{\text{vac}}} + \underbrace{\sqrt{2} G_F N_e \begin{pmatrix} 1 & & \\ & 0 & \\ & & 0 \end{pmatrix}}_{H_{\text{mat}}} + \underbrace{\begin{pmatrix} a_{ee} & a_{e\mu} & a_{e\tau} \\ a_{e\mu}^* & a_{\mu\mu} & a_{\mu\tau} \\ a_{e\tau}^* & a_{\mu\tau}^* & a_{\tau\tau} \end{pmatrix}}_{H_{\text{LIV}}} \\ &= \frac{1}{2E} U \begin{pmatrix} 0 & 0 & 0 \\ 0 & \Delta m_{21}^2 & 0 \\ 0 & 0 & \Delta m_{31}^2 \end{pmatrix} U^\dagger + \sqrt{2} G_F N_e \begin{pmatrix} 1 & & \\ & 0 & \\ & & 0 \end{pmatrix} + \begin{pmatrix} a_{ee} - a_{\tau\tau} & a_{e\mu} & a_{e\tau} \\ a_{e\mu}^* & a_{\mu\mu} - a_{\tau\tau} & a_{\mu\tau} \\ a_{e\tau}^* & a_{\mu\tau}^* & 0 \end{pmatrix}. \end{aligned} \quad (2.4)$$

The first term containing the usual leptonic mixing matrix U and the neutrino mass eigenstates $m_i (i = 1, 2, 3)$ is the standard vacuum hamiltonian. The second term, proportional

²The presence of LIV makes it necessary to report the LIV bounds in a specific frame to conveniently compare the results from various experiments. Following the widely used practice in literature, the LIV coefficients used in our analysis are defined in the Sun-centered celestial equatorial frame. The Z direction points north along the earth's rotational axis, X direction points towards the vernal equinox, while the Y direction completes the right-handed coordinate system [70]. Observations performed in any other inertial frame of reference can be related to that in this Sun-centered frame via Lorentz transformations. We refer the reader to reference [73] for more details on LIV-related measurements performed in other frames of reference and how they can be related to the standard Sun-centered celestial frame of reference.

to Fermi constant G_F and electron density N_e along the neutrino propagation, originates from standard charged-current coherent forward scattering of neutrinos with electrons in earth matter. The third term containing the LIV parameters $a_{\alpha\beta}$'s ($\alpha, \beta = e, \mu, \tau$) incorporates the effect of LIV (and also CPT-violation). The off-diagonal $a_{\alpha\beta}$'s ($\alpha \neq \beta$) are complex with a phase ($\varphi_{\alpha\beta}$) associated to them, while the diagonal parameters are real. As per convention, in the second line of Eq. 2.4, a common term (m_1^2) has been subtracted from the diagonal elements in H_{vac} , and another common term $a_{\tau\tau}$ has been subtracted from the diagonal elements of H_{LIV} . Both of these subtractions have the effect of removing an overall phase factor, which will have no impact on the oscillation probabilities. This implies that neutrino oscillation can effectively probe only two of the three diagonal parameters in H_{LIV} . In our analysis, those two parameters are $\tilde{a}_{ee} = a_{ee} - a_{\tau\tau}$ & $\tilde{a}_{\mu\mu} = a_{\mu\mu} - a_{\tau\tau}$, while the individual value of $a_{\tau\tau}$ cannot be probed by the oscillation experiment. Thus for simplicity we take $a_{\tau\tau}$ to be zero and thus $\tilde{a}_{ee} = a_{ee}$, and $\tilde{a}_{\mu\mu} = a_{\mu\mu}$. Note that, any one of the three diagonal LIV parameters can be chosen to be removed from the analysis in this way.

It is worthwhile to mention here that the physics of neutral current (NC) Nonstandard interaction (NSI) (usually denoted by $\varepsilon_{\alpha\beta}$) that arises from neutrino mass models and introduces couplings between the neutrinos and the first generation fermions e, u, d , has an apparent similarity with the form of LIV hamiltonian, - thereby suggesting a mathematical mapping: $\varepsilon_{\alpha\beta} \leftrightarrow a_{\alpha\beta}/\sqrt{2}G_F N_e$. But there is a crucial difference between these two different kinds of physics scenario as discussed in detail in reference [75]. NC NSI is proportional to the density along the neutrino trajectory and is thus very tiny for short-baseline neutrino experiments. LIV, on the other hand, is an intrinsic effect that is present even in the vacuum.

3 Impact of LIV parameters on probability

In this work we focus on $a_{\alpha\beta}$'s and we will now describe how they affect the oscillation probability expressions in various channels. Since the main contribution comes from the $\nu_\mu \rightarrow \nu_e$ oscillation channel, we discuss about how $P(\nu_\mu \rightarrow \nu_e)$ is affected by LIV. The most important LIV parameters impacting this channel are $a_{e\mu}$ and $a_{e\tau}$, and also to a lesser extent a_{ee} . Following the similar approach as in reference [43, 76–78], we can approximately write the $\nu_\mu \rightarrow \nu_e$ oscillation probability as the sum of the following three terms,

$$P_{\mu e}(\text{SI}+\text{LIV}) \simeq P_{\mu e}(\text{SI}) + P_{\mu e}(a_{e\mu}) + P_{\mu e}(a_{e\tau}), \quad (3.1)$$

where the first term on the right hand side is the probability term corresponding to standard interaction (SI) with earth matter, while the other two terms come due to the presence of LIV parameters $a_{e\mu}$ and $a_{e\tau}$. The three terms on the right hand side can be shown to have the following forms.

$$P_{\mu e}(\text{SI}) \simeq X + Y \cos(\delta_{13} + \Delta), \quad (3.2)$$

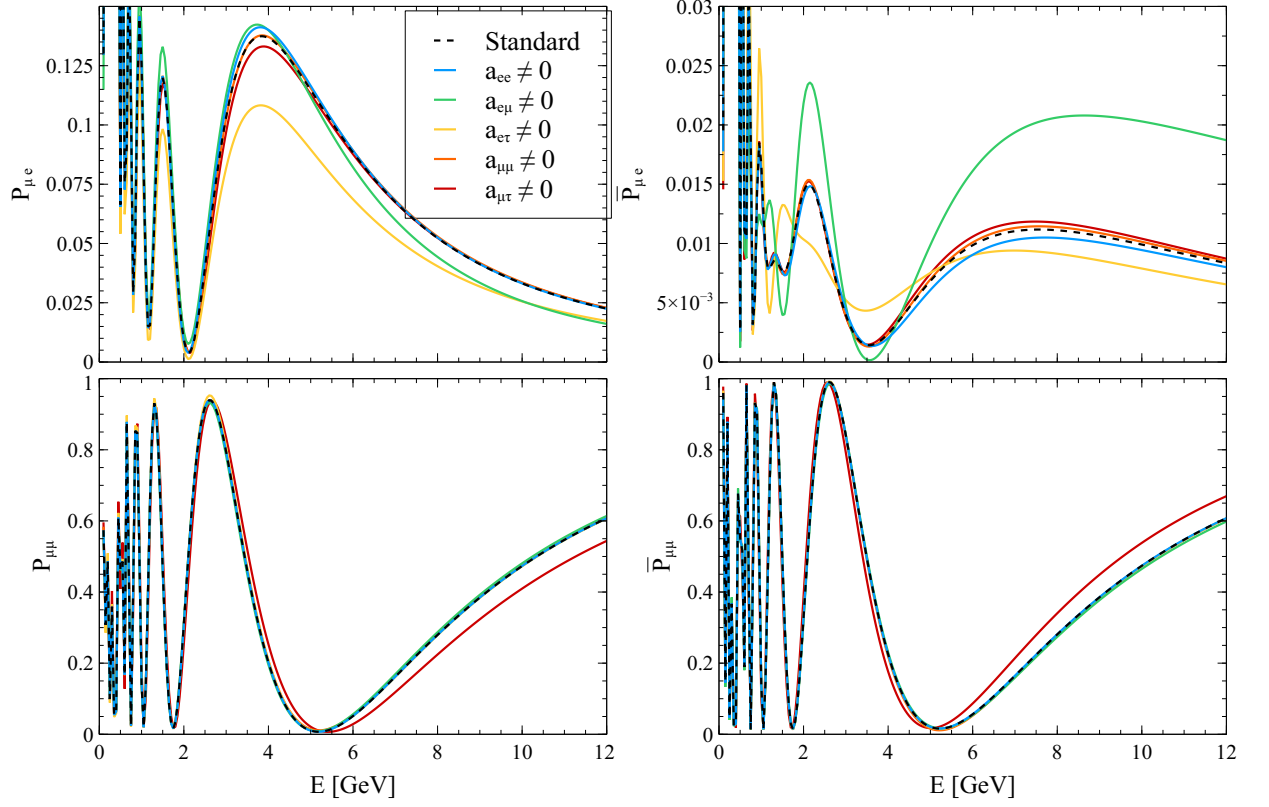


Figure 1. The impact of individual LIV parameters on oscillation probability at the P2O baseline of 2595 km. The top (bottom) row shows the probability for appearance (disappearance) channel, while the left (right) column indicates the neutrino (anti-neutrino) mode. The black dotted curve shows the probability for the standard (no LIV) case, while the solid coloured curves are for individual LIV parameters present. The non-zero values of the individual LIV parameters $a_{\alpha\beta}$ was taken as 5×10^{-23} GeV, while the CP phase associated with the off-diagonal LIV parameters was taken as zero.

$$\begin{aligned}
& P_{\mu e}(a_{e\mu}) \\
& \simeq \frac{8|a_{e\mu}|E\Delta s_{13} \sin 2\theta_{23} c_{23} \sin \Delta}{\Delta m_{31}^2} \left[-\sin \Delta \sin(\delta_{13} + \varphi_{e\mu}) + \left(\frac{s_{23}^2}{c_{23}^2} \frac{\sin \Delta}{\Delta} + \cos \Delta \right) \cos(\delta_{13} + \varphi_{e\mu}) \right],
\end{aligned} \tag{3.3}$$

$$\begin{aligned}
& P_{\mu e}(a_{e\tau}) \\
& \simeq \frac{8|a_{e\tau}|E\Delta s_{13} \sin 2\theta_{23} s_{23} \sin \Delta}{\Delta m_{31}^2} \left[\sin \Delta \sin(\delta_{13} + \varphi_{e\tau}) + \left(\frac{\sin \Delta}{\Delta} - \cos \Delta \right) \cos(\delta_{13} + \varphi_{e\tau}) \right].
\end{aligned} \tag{3.4}$$

The different familiar terms appearing in Eqs. 3.2, 3.3, 3.4 are given in the following.

$$\begin{aligned}
X &= 4s_{13}^2 c_{13}^2 s_{23}^2 \frac{\sin^2 [(1 - \hat{A})\Delta]}{(1 - \hat{A})^2}; & Y &= 8\alpha s_{12} c_{12} s_{23} c_{23} s_{13} c_{13} \frac{\sin \hat{A} \Delta \sin [(1 - \hat{A})\Delta]}{\hat{A} (1 - \hat{A})}, \\
\hat{A} &= \frac{2\sqrt{2}G_F N_e E}{\Delta m_{31}^2}; & \Delta &= \frac{\Delta m_{31}^2 L}{4E}; & s_{ij} &= \sin \theta_{ij}; & c_{ij} &= \cos \theta_{ij}; & \alpha &= \frac{\Delta m_{21}^2}{\Delta m_{31}^2}.
\end{aligned}
\tag{3.5}$$

In presence of a_{ee} , the replacement $\hat{A} \rightarrow \hat{A}[1 + a_{ee}/\sqrt{2}G_F N_e] \simeq \hat{A} + a_{ee}/(2E/\Delta m_{31}^2)$ has to be made. In order to understand the impact of the LIV parameters, we first have a look at the oscillation probability at the P2O baseline of 2595 km. This was estimated numerically using the widely used General Long Baseline Experiment Simulator (GLoBES) [79, 80] and the associated package *snu.c* [81, 82] with necessary modifications. We consider Normal mass ordering (NO) and take the following best fit values [8] of the oscillation parameters: $\theta_{12} = 34.3^\circ, \theta_{13} = 8.58^\circ, \theta_{23} = 48.8^\circ, \delta_{13} = -0.68\pi, \Delta m_{21}^2 = 7.5 \times 10^{-5} \text{ eV}^2, \Delta m_{31}^2 = 2.5 \times 10^{-3} \text{ eV}^2$. We take one LIV parameter $a_{\alpha\beta}$ non-zero (fixed at the same numerical value of $5 \times 10^{-23} \text{ GeV}$, and the associated CP phase $\varphi_{\alpha\beta} = 0$) at a time to assess the role of individual LIV parameters in the probability level, and show the results in Fig. 1.

As expected, the appearance channel is most affected by the LIV parameters $a_{e\mu}$ and $a_{e\tau}$. Compared to the standard case (black dashed curve), $a_{e\mu}$ increases the magnitude of $P(\nu_\mu \rightarrow \nu_e)$ while the presence of $a_{e\tau}$ shows a depletion around the oscillation maxima of 4–5 GeV. This is due to the fact that both the $\sin \delta_{13}$ and $\cos \delta_{13}$ terms within the square brackets of Eq. 3.4 have the same sign (negative, thus decreasing $P_{\mu e}$), while there is a relative sign between two such terms in Eq. 3.3, - thus leading to a smaller enhancement of $P_{\mu e}$. The effects of $a_{e\mu}$ and $a_{e\tau}$ become qualitatively opposite for the $P_{\bar{\nu}_\mu \rightarrow \bar{\nu}_e}$ channel. We also observe that a_{ee} increases or decreases the probabilities only mildly. The disappearance channel, on the other hand is impacted by only the parameters $a_{\mu\mu}$ and $a_{\mu\tau}$, - the changes induced by them being in the opposite direction for ν and $\bar{\nu}$ -modes.

The sensitivity to the LIV parameters depends on the change in probability due to the presence of LIV:

$$\Delta P_{\alpha\beta} = P_{\alpha\beta}(\text{SI+LIV}) - P_{\alpha\beta}(\text{SI}), \quad (\alpha, \beta = e, \mu, \tau). \tag{3.6}$$

In order to have an approximate idea about the physics behind the sensitivity estimates, we focus on the dominant channel, *i.e.*, the $\nu_\mu \rightarrow \nu_e$ channel and the most relevant LIV parameters $a_{e\mu}, a_{e\tau}, a_{ee}$.

In Fig. 2 we show by means of a heatmap, how the absolute difference $|\Delta P_{\mu e}|$ evolves with variation in the LIV parameters and the variation in the standard CP phase δ_{13} , for a fixed baseline and energy. In top (bottom) row, we consider the baseline 2595 (1300) km and approximate first oscillation maximum energy 5 (2.5) GeV for the P2O (DUNE) experiment. The light yellow end of the colour spectrum corresponds to lower $|\Delta P_{\mu e}|$ (*i.e.*, more degeneracy between SI and LIV), while the darker shades indicate a higher impact of the corresponding LIV parameter, resulting in a higher value of $|\Delta P_{\mu e}|$.

In all the heatplots we see that there is little to no change in the probability for very small values of the LIV parameter, which is consistent with our expectation. In

presence of $a_{e\mu}$ ($a_{e\tau}$), we note the presence of a set of two degenerate (yellow) *branches* appearing at two different values of δ_{13} . Interestingly these degeneracies remain present irrespective of the values of $|a_{e\mu}|$ or $|a_{e\tau}|$ and the degenerate regions are almost parallel to the LIV parameter axis. These features are more prominent for the P2O baseline than the DUNE baseline. On the other hand, in presence of a_{ee} , P2O baseline shows an additional degeneracy approximately around $a_{ee} \simeq 22 \times 10^{-23}$ GeV, but curiously this is absent for DUNE.

For an analytical understanding of the various features, we use Eqs. 3.1, 3.2, 3.3, 3.4 to express $|\Delta P_{\mu e}|$ in presence of $a_{e\mu}$ or $a_{e\tau}$ as the following.

$$\Delta P_{\mu e}(|a_{e\mu}|) \simeq 8|a_{e\mu}| \frac{\pi}{2} E s_{13} \sin 2\theta_{23} c_{23} \left[-\sin \delta_{13} + \frac{2}{\pi} \frac{s_{23}^2}{c_{23}^2} \cos \delta_{13} \right], \quad (3.7)$$

$$\Delta P_{\mu e}(|a_{e\tau}|) \simeq 8|a_{e\tau}| \frac{\pi}{2} E s_{13} \sin 2\theta_{23} s_{23} \left[\sin \delta_{13} + \frac{2}{\pi} \cos \delta_{13} \right]. \quad (3.8)$$

Note that, since all the heatplots are generated corresponding to the first oscillation maximum, we put $\Delta = \Delta m_{31}^2 \cdot L/E \simeq \pi/2$ in deriving Eqs. 3.7 and 3.8. $\Delta P_{\mu e}(|a_{e\mu}|)$ (or $\Delta P_{\mu e}(|a_{e\tau}|)$) is directly proportional to $|a_{e\mu}|$ (or $|a_{e\tau}|$) respectively, - which clearly shows

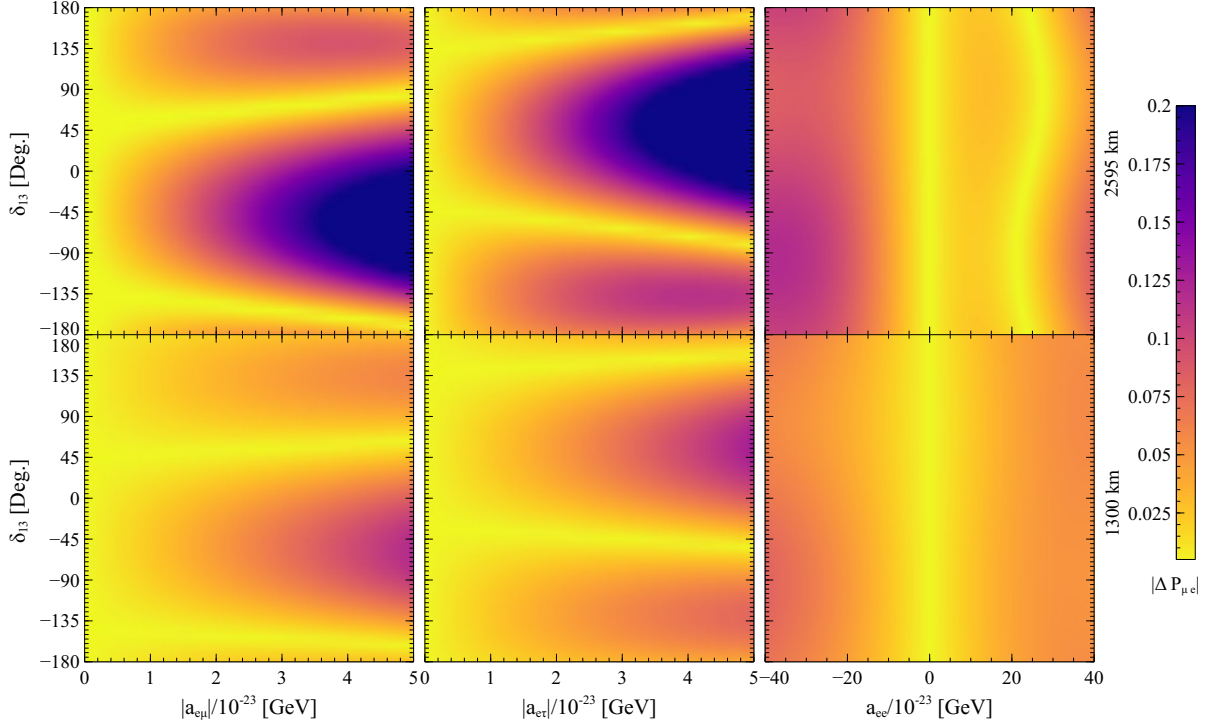


Figure 2. We plot the heatplot for $|\Delta P_{\mu e}| = |P_{\mu e}(\text{SI+LIV}) - P_{\mu e}(\text{SI})|$ for the P2O baseline of 2595 km (top row) and for DUNE baseline of 1300 km (bottom row). The plots were done for the respective values of energies roughly corresponding to first oscillation maximum: 2.5 GeV for DUNE and 5 GeV for P2O. The heatplot is shown as a function of the three LIV parameters ($|a_{e\mu}|, |a_{e\tau}|, a_{ee}$) along the horizontal axes and the standard (Dirac) CP phase δ_{13} .

that for very small values of the LIV parameters, we get a degeneracy. For the pair of yellow degenerate *branches* in the first two columns of Fig. 2, the quantities inside the square brackets of Eqs. 3.7 and 3.8 need to vanish, and the solutions are independent of the value of the LIV parameter and the baseline. For the case of $|a_{e\mu}|$, this condition becomes,

$$\sin \delta_{13} = \frac{2}{\pi} \frac{s_{23}^2}{c_{23}^2} \cos \delta_{13}. \quad (3.9)$$

Putting $\theta_{23} = 48.8^\circ$, the solutions are $\delta_{13} \simeq 39^\circ, -141^\circ$. It is clear from the $(s_{23}/c_{23})^2$ factor that for θ_{23} lying in the higher octant, first solution for δ_{13} will move (mildly) closer to $\pi/4$, making the second solution move towards $-\pi/4$. For the case of $|a_{e\tau}|$, using Eq. 3.8 the degenerate condition translates to,

$$\sin \delta_{13} = -\frac{2}{\pi} \cos \delta_{13}, \quad (3.10)$$

the solutions of which are given by roughly $\delta_{13} \simeq -33^\circ, 147^\circ$. We note that the solutions for δ_{13} for Eqs. 3.9 and 3.10 for the locations of degeneracies approximately differ by a sign (as long as θ_{23} does not lie too far from the maximal value of $\pi/4$), or equivalently they differ by a $\pm\pi/2$ phase-shift. These locations of degeneracies and the shift of the solutions for $|a_{e\mu}|$ and $|a_{e\tau}|$ are consistent with Fig. 2. The slight *slanting* nature of the degenerate branches with increase in $|a_{e\mu}|$ originates due to subdominant higher order terms, which we have not considered in our simplified analysis. In Fig. 2, we note that deviation from the standard case happens more quickly when the CP phase $\delta_{13} \in [-\pi/2, 0]$ (for $|a_{e\mu}|$) and $\delta_{13} \in [0, \pi/2]$ (for $|a_{e\tau}|$), - manifested by the presence of darker patches around $|a_{e\mu}|$ or $|a_{e\tau}| \gtrsim 2 \times 10^{-23}$ GeV. These two separate quadrants for δ_{13} originate due to the presence of the relative sign between the $\sin \delta_{13}$ and $\cos \delta_{13}$ terms inside the square brackets in Eqs. 3.7 and 3.8. The proportionality of Eqs. 3.7 and 3.8 with energy suggests that the features are quantitatively more prominent for P2O than DUNE, since the peak energy corresponding to the former is twice the latter (5 GeV, as compared to 2.5 GeV for DUNE). To understand the features induced by the presence of a_{ee} , we deduce the corresponding probability difference as follows (using Eq. 3.2 and replacing $\hat{A} \rightarrow \hat{A}[1 + a_{ee}/\sqrt{2}G_F N_e]$ to account for a_{ee}).

$$\Delta P_{\mu e}(a_{ee}) \simeq 4s_{13}^2 c_{13}^2 s_{23}^2 \left\{ \frac{\sin^2 [1 - \hat{A}(1 + a_{ee}/\sqrt{2}G_F N_e)] \Delta}{[1 - \hat{A}(1 + a_{ee}/\sqrt{2}G_F N_e)]^2} - \frac{\sin^2 [1 - \hat{A}] \Delta}{[1 - \hat{A}]^2} \right\} + \cos \delta_{13}\text{-term}. \quad (3.11)$$

The $\cos \delta_{13}$ -term containing Y from Eq. 3.2 is suppressed by a factor α ($= \Delta m_{21}^2 / \Delta m_{31}^2 \sim 10^{-2}$) compared to the first term in Eq. 3.11. We neglect this term for simplicity. Thus the degeneracy condition ($\Delta P_{\mu e}(a_{ee}) \simeq 0$) in presence of a_{ee} can be simplified to the following equation.

$$\underbrace{\left[\frac{\sin [1 - \hat{A}(1 + \hat{a}_{ee})] \Delta}{1 - \hat{A}(1 + \hat{a}_{ee})} - \frac{\sin [1 - \hat{A}] \Delta}{1 - \hat{A}} \right]}_{I_-} \times \underbrace{\left[\frac{\sin [1 - \hat{A}(1 + \hat{a}_{ee})] \Delta}{1 - \hat{A}(1 + \hat{a}_{ee})} + \frac{\sin [1 - \hat{A}] \Delta}{1 - \hat{A}} \right]}_{I_+} = 0, \quad (3.12)$$

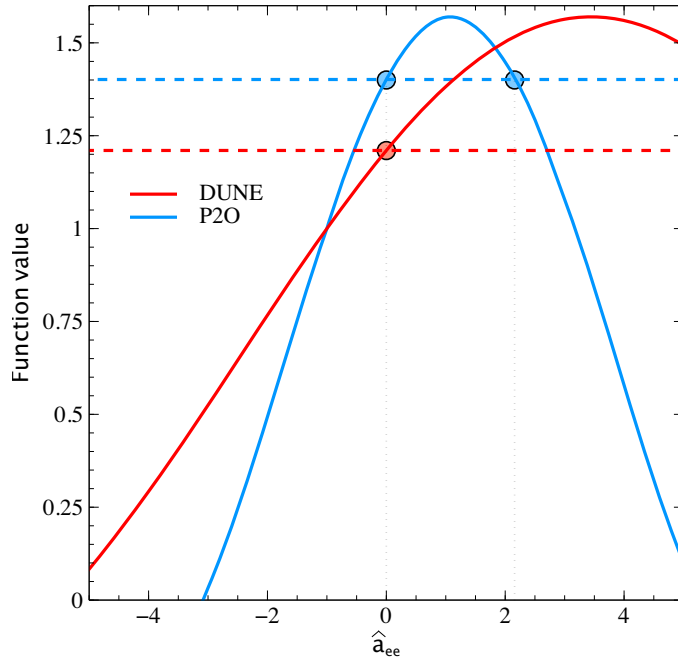


Figure 3. The two terms in I_- from Eq. 3.12 are plotted for both DUNE (red) and P2O (blue) as functions of the parameter $\hat{a}_{ee} = a_{ee}/\sqrt{2}G_F N_e$. The solid curve is the first term ($\frac{\sin[1-\hat{A}(1+\hat{a}_{ee})]\Delta}{1-\hat{A}(1+\hat{a}_{ee})}$), while the dashed curve is the second term ($\frac{\sin[1-\hat{A}]\Delta}{1-\hat{A}}$). The small coloured circles show the locations of solutions where the two terms intersect.

where $\hat{a}_{ee} = a_{ee}/\sqrt{2}G_F N_e$. It is easy to see that I_+ cannot be zero, and for I_- to vanish we can immediately identify $a_{ee} = 0$ as the trivial solution. To examine the possibility of further degeneracies, we note the following.

$$\Delta \simeq \pi/2; \quad (\text{for both P2O and DUNE})$$

$$\hat{A} \simeq \frac{2\sqrt{2}G_F N_e E}{\Delta m_{31}^2} \simeq 0.03 \times \rho[\text{g.cm}^{-3}] \times E[\text{GeV}] \simeq \begin{cases} 0.225, & (\text{for DUNE, } \rho \simeq 3, E \simeq 2.5) \\ 0.448. & (\text{for P2O, } \rho \simeq 3.2, E \simeq 5). \end{cases} \quad (3.13)$$

To find other solutions when $I_- = 0$, we plot the two terms in I_- for both DUNE and P2O as a function of the parameter \hat{a}_{ee} in Fig. 3. The first term is an oscillating function of \hat{a}_{ee} , while the second term is a constant. For DUNE, having a lower baseline and energy, the *sine* function (red solid) oscillates slowly and has only the trivial solution in the range shown. Corresponding *sine* function for P2O (blue solid) oscillates faster, given the larger baseline and energy, and thus can have a second (non-trivial) solution at a reasonably smaller positive value of $\hat{a}_{ee} \simeq 2.2$, which translates to $a_{ee} = 2.2\sqrt{2}G_F N_e \simeq 24.8 \times 10^{-23}$ GeV. This is almost exactly the location of the second degeneracy in the top right panel of Fig. 2. The mild dependence of this degeneracy branch on the CP phase δ_{13} arises from the $\cos\delta_{13}$ -term in Eq. 3.11 which we have neglected for simplicity.

In Fig. 4, we show the heatmap for $|\Delta P_{\mu e}|$ in the parameter space of θ_{23} and one LIV parameter ($|a_{e\mu}|, |a_{e\tau}|, a_{ee}$), for a fixed CP phase $\delta_{13} = -0.68\pi$. Comparing the first and

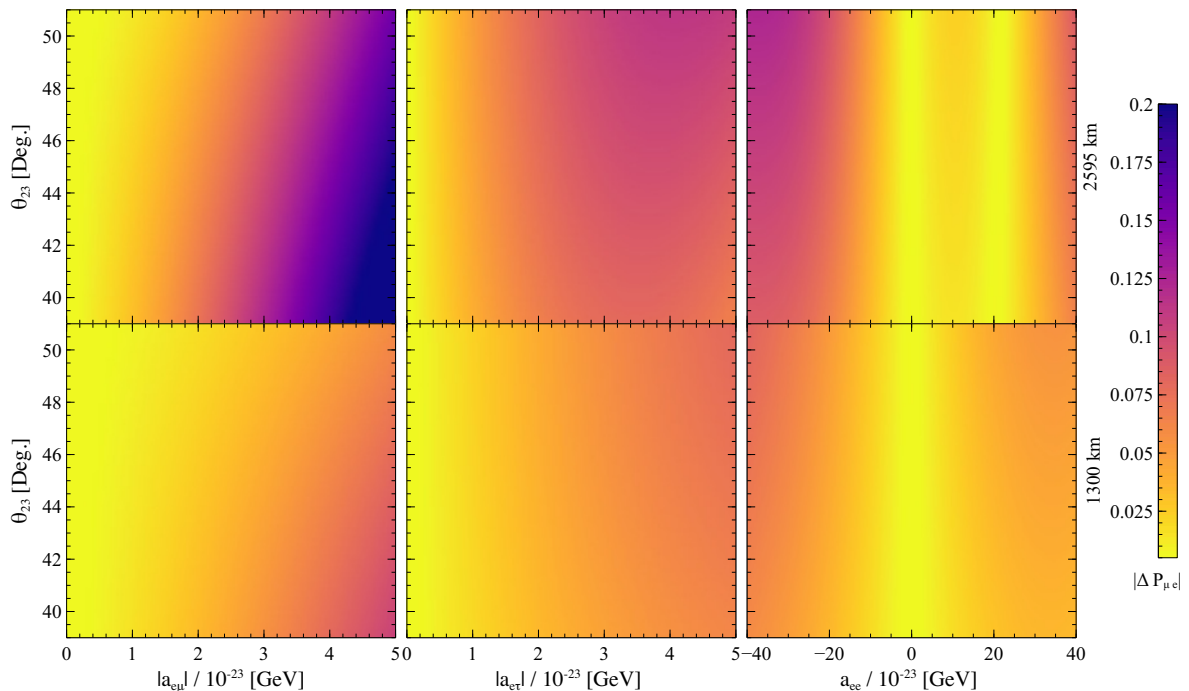


Figure 4. Similar to Fig. 2 but shown as a function of θ_{23} with fixed δ_{13} .

the middle columns, we see that $a_{e\mu}$ has a slightly bigger impact than $a_{e\tau}$. Moreover, presence of $a_{e\mu}$ induces more deviation at lower octant (LO), while that of $a_{e\tau}$ is apparent at higher octant (HO). If we look at the analytical expressions for $\Delta P_{\mu e}$ in Eqs. 3.7 and 3.8, this octant dependence originates due to the overall factor c_{23} in presence of $a_{e\mu}$ and s_{23} in presence of $a_{e\tau}$ (note that the factor $\sin 2\theta_{23}$ in those equations are octant-independent). In the third column of Fig. 4, a_{ee} again gives rise to additional degeneracy for P2O, which has already been explained above with regard to Fig. 2.

4 Simulation details

We simulate the long baseline neutrino experiments DUNE and P2O using GLoBES [79, 80] and use the add-on *snu.c* [81, 82] to implement the physics of LIV. DUNE is a 1300 km long baseline experiment from the accelerator at the site of FermiLab to the site employing a liquid argon far detector (FD) of 40 kt fiducial mass at South Dakota. The experiment is capable of using a proton beam of power 1.07 MW and of running 3.5 years each on ν and $\bar{\nu}$ mode (resulting in a total exposure of roughly 300 kt.MW.yr corresponding to total 1.47×10^{21} protons on target or POT). The flux, cross-sections, migration matrices for energy reconstruction, efficiencies *etc.* were implemented according to the official configuration files [83] provided by the DUNE collaboration for its simulation.

P2O (Protvino to ORCA) is a proposed long baseline neutrino experiment with a baseline of nearly 2595 km from the Protvino accelerator complex, situated at 100 km south

of Moscow to the site of ORCA (Oscillation Research with Cosmics in the Abyss), hosting 6 MT Cerenkov detector located 40 km off the coast in South France, at a mooring depth of 2450 m in the Mediterranean sea. ORCA is the low energy component of the KM3NeT Consortium [84], with a primary goal of studying atmospheric neutrino oscillations in the energy range of 3 to 100 GeV in order to determine the neutrino mass ordering. Currently, 10 lines (*i.e.*, detection units) of the ORCA detector are live and taking data. A full ORCA detector is expected to have 115 lines and foresees completion in subsequent phases around 2025 [85]. Construction of the neutrino beamline and relevant upgradation of the accelerator for the P2O experiment is expected to be completed in a few years. Assuming a favorable geopolitical situation and available funding, the P2O project in its nominal configuration might be realised during the next decade [86]. We simulate the nominal configuration³ of P2O experiment using a 90 kW proton beam with a runtime of 3 yrs. in ν and 3 yrs. in $\bar{\nu}$ mode, - corresponding to a total POT of 4.8×10^{20} . The baseline mostly passes through the upper mantle of the earth with an average density of 3.4 g/cc and the deepest point along the beam being 134 km [87]. The fluxes, detector response parameters, the detection efficiencies, signal and background systematics *etc.*, corresponding to our nominal P2O configuration were taken from [18, 84].

To estimate the sensitivity of LBL experiments to probe the LIV parameters, we carry out a $\Delta\chi^2$ analysis using GLOBES. The analytical⁴ form of the $\Delta\chi^2$ can be expressed as,

$$\Delta\chi^2(p^{\text{true}}) = \text{Min}_{p^{\text{test}}, \eta} \left[2 \sum_k^{\text{mode}} \sum_j^{\text{channel}} \sum_i^{\text{bin}} \left\{ N_{ijk}^{\text{test}}(p^{\text{test}}; \eta) - N_{ijk}^{\text{true}}(p^{\text{true}}) + N_{ijk}^{\text{true}}(p^{\text{true}}) \ln \frac{N_{ijk}^{\text{true}}(p^{\text{true}})}{N_{ijk}^{\text{test}}(p^{\text{test}}; \eta)} \right\} + \sum_l \frac{(p_l^{\text{true}} - p_l^{\text{test}})^2}{\sigma_{p_l}^2} + \sum_m \frac{\eta_m^2}{\sigma_{\eta_m}^2} \right]. \quad (4.1)$$

N^{true} corresponds to the simulated set of event spectra corresponding to *true* set of oscillation parameters p^{true} , where only standard scenario is assumed with all the LIV parameters $a_{\alpha\beta}$ ($\alpha, \beta = e, \mu, \tau$) kept fixed to zero and all the standard oscillation parameters are kept fixed to their bestfit values. N^{test} denotes the events simulated in presence of LIV, where the LIV parameters, as well as some of the less well-measured standard oscillation parameters are allowed to vary. The total set of standard and LIV parameters that generate N^{test} are denoted by p^{test} . Table 1 summarizes the values of the standard and LIV oscillation parameters used in our analysis. Note that in generating N^{test} we have kept the three well-measured standard parameters $\theta_{12}, \theta_{13}, \Delta m_{21}^2$ fixed to their bestfit values. We have checked that varying these three parameters in the fit produces negligible changes to the result. We varied the other three less well-measured standard parameters $\theta_{23}, \Delta m_{31}^2, \delta_{13}$, as well as the LIV parameters $|a_{\alpha\beta}|, \varphi_{\alpha\beta}$ ($\alpha, \beta = e, \mu, \tau$). Throughout the analysis we assume the *true* mass hierarchy to be normal and vary the *test* value of Δm_{31}^2 over both the normal

³There are proposals for using an upgraded proton beam with 450 kW power and also to use the Super-ORCA detector with denser geometry, lower energy thresholds and better flavour identification capabilities [18].

⁴This is the *Poissonian* definition of $\Delta\chi^2$, which in the limit of large sample size, reduces to the Gaussian form.

Fixed/Varied	Parameter	Bestfit/true value (p^{true})	Variation range (3σ interval) (p^{test})	1σ uncertainty (prior) (σ_{pl})
Fixed	θ_{12} [Deg.]	34.3	[31.4, 37.4]	-
	θ_{13} [Deg.]	8.53	[8.16, 8.94]	-
	Δm_{21}^2 [10^{-5} eV ²]	7.5	[6.94, 8.14]	-
Varied	θ_{23} [Deg.]	48.8	[41.63, 51.32]	3.5%
	Δm_{31}^2 [10^{-3} eV ²]	2.55	[2.46, 2.65] \cup [-2.55, -2.37]	2.4%
	δ_{13} [Deg.]	-122.4	[-180, 0] \cup [144, 180]	-
	a_{ee} [10^{-23} GeV]	0	[-40, 40]	-
	$a_{\mu\mu}$ [10^{-23} GeV]	0	[-10, 10]	-
	$ a_{e\mu} $ [10^{-23} GeV]	0	[0, 5]	-
	$ a_{e\tau} $ [10^{-23} GeV]	0	[0, 5]	-
	$ a_{\mu\tau} $ [10^{-23} GeV]	0	[0, 5]	-
	$\varphi_{e\mu}$ [Deg.]	0	[-180, 180]	-
	$\varphi_{e\tau}$ [Deg.]	0	[-180, 180]	-
	$\varphi_{\mu\tau}$ [Deg.]	0	[-180, 180]	-

Table 1. The values of standard and LIV parameters used in our study. The first column indicates whether the parameters were kept fixed or varied around their true values. The third column shows the *true* values used (taken from the globalfit analysis in [8]), while the next column shows the range of variation (taken to be the current 3σ interval). The rightmost column shows the prior uncertainties used while varying the corresponding parameters in the analysis. If the 3σ upper and lower limit of a parameter is x_u and x_l respectively, the 1σ uncertainty is $(x_u - x_l)/3(x_u + x_l)\%$ [13].

and inverted hierarchy. The sums over the three indices i, j, k signify the summations over the energy bins, the oscillation channels (ν_e appearance and ν_μ disappearance), and the running modes (neutrino and antineutrino modes) respectively. For DUNE we take a total of 71 energy bins in the range of 0 – 20 GeV, - with 64 bins with uniform widths of 0.125 GeV in the energy range of 0 to 8 GeV and 7 bins with varying widths beyond 8 GeV [83]. For P2O, we take 40 uniform bins up to 12 GeV. Thus the first term ($N^{\text{test}} - N^{\text{true}}$) inside the curly braces accounts for the algebraic difference between the two sets of data, whereas the log-term gives a kind of fractional difference between them. The entire expression in the curly brackets with summations over i, j, k consists of the statistical part of the $\Delta\chi^2$.

Uncertainties in the prior measurement of the l^{th} oscillation parameter are given by the parameters σ_{pl} . As indicated in Table 1, for the variation of θ_{23} and Δm_{31}^2 , we have used prior uncertainties of 3.5% and 2.4% respectively⁵. For Δm_{31}^2 we have varied over the sign also to take care of the possible fake solutions in the opposite mass hierarchy. We have allowed the rest of the parameters $\delta_{13}, a_{ee}, a_{\mu\mu}, |a_{e\mu}|, |a_{e\tau}|, |a_{\mu\tau}|, \varphi_{e\mu}, \varphi_{e\tau}, \varphi_{\mu\tau}$ to vary in an unrestricted manner without any prior uncertainties. η_m is the nuisance parameter/systematics and σ_{η_m} is the corresponding uncertainty which arises from the detector properties. Table 2 summarizes the overall normalization uncertainties of these systematic parameters for various signals and backgrounds used in our analysis. We assume the various signal and background systematic parameters are distributed in a Gaussian way

⁵Due to the degenerate solutions existing in two octant of θ_{23} , we have also checked some of our subsequent results by increasing the prior uncertainty of θ_{23} to values higher than 3.5%, such that the *test* θ_{23} -values span both the octants. We found that as long as the prior is not too high ($\lesssim 15\%$), the results do not change significantly.

Systematics /Nuisance parameters (η)	Uncertainty (σ_η) (DUNE)	Uncertainty (σ_η) (P2O)
ν_e signal normalization	2%	5%
$\bar{\nu}_e$ signal normalization	2%	5%
ν_μ signal normalization	5%	5%
$\bar{\nu}_\mu$ signal normalization	5%	10%
ν_e background normalization	5%	10%
$\bar{\nu}_e$ background normalization	5%	10%
ν_μ background normalization	5%	10%
$\bar{\nu}_\mu$ background normalization	5%	10%
Neutral current background normalization	10%	10%
ν_τ background normalization	20%	20%
$\bar{\nu}_\tau$ background normalization	20%	20%
Density	10%	10%

Table 2. The signal/ background systematics and the density uncertainties used in our analysis for both DUNE and P2O configurations.

with mean value 0 and standard deviation σ_{η_m} , indicated in the second and third columns of Table 2 for DUNE and P2O respectively. This way of treating the systematics in the $\Delta\chi^2$ calculation is known as the *method of pulls* [88–91]. The background normalization uncertainties include correlations among various sources of backgrounds (contamination of $\nu_e/\bar{\nu}_e$ in the incident beam, flavour misidentification, neutral current, and ν_τ). We further include a 10% prior uncertainty on both the baseline densities of DUNE (2.95 g/cc) and P2O (3.4 g/cc). The final estimate of the (minimum) $\Delta\chi^2$ is obtained after varying the relevant oscillation parameters (as mentioned earlier and summarized in Table 1 and the systematic parameters along with the densities (see Table 2), and reporting the minimum value of the $\Delta\chi^2$. The procedure is known as the marginalization of the relevant oscillation parameters so that the final result gives a conservative estimate of $\Delta\chi^2$. The $\Delta\chi^2$ thus estimated is the frequentist method of hypotheses testing [89, 92].

5 Correlations among the LIV parameters

In Fig. 5, we show the 95% confidence level (C.L.) regions in the parameters space spanned by one off-diagonal LIV parameter $|a_{\alpha\beta}|$ ($|a_{e\mu}|$, $|a_{e\tau}|$ or $|a_{\mu\tau}|$) and one diagonal LIV parameter $a_{\alpha'\beta'}$ (a_{ee} or $a_{\mu\mu}$). Thus we assume the presence of two LIV parameters at a time in the fit. The three standard parameters as well as the relevant LIV phases are then varied (see Table 1) and to obtain the minimum $\Delta\chi^2$ (*i.e.*, we marginalize over the three standard parameters and the LIV CP phases.). For instance, for the analysis in the parameter space of $a_{ee} - |a_{e\mu}|$, we vary $\theta_{23}, \Delta m_{31}^2$ (sign and magnitude) with priors 3.5% and 2.4% respectively and $\delta_{13}, \varphi_{e\mu}$ without priors in an unrestricted manner and obtain the minimum $\Delta\chi^2$ as a function of a_{ee} and $|a_{e\mu}|$. We repeat the procedure for many sets of $(a_{ee}, |a_{e\mu}|)$ to plot the iso- $\Delta\chi^2$ contours at a C.L. of 95% (which corresponds to a $\Delta\chi^2$ value of 5.99 for 2 d.o.f.). The blue contours show the sensitivity reach of P2O alone while the red ones illustrate the results of combining the projected data of P2O and DUNE (which we write as

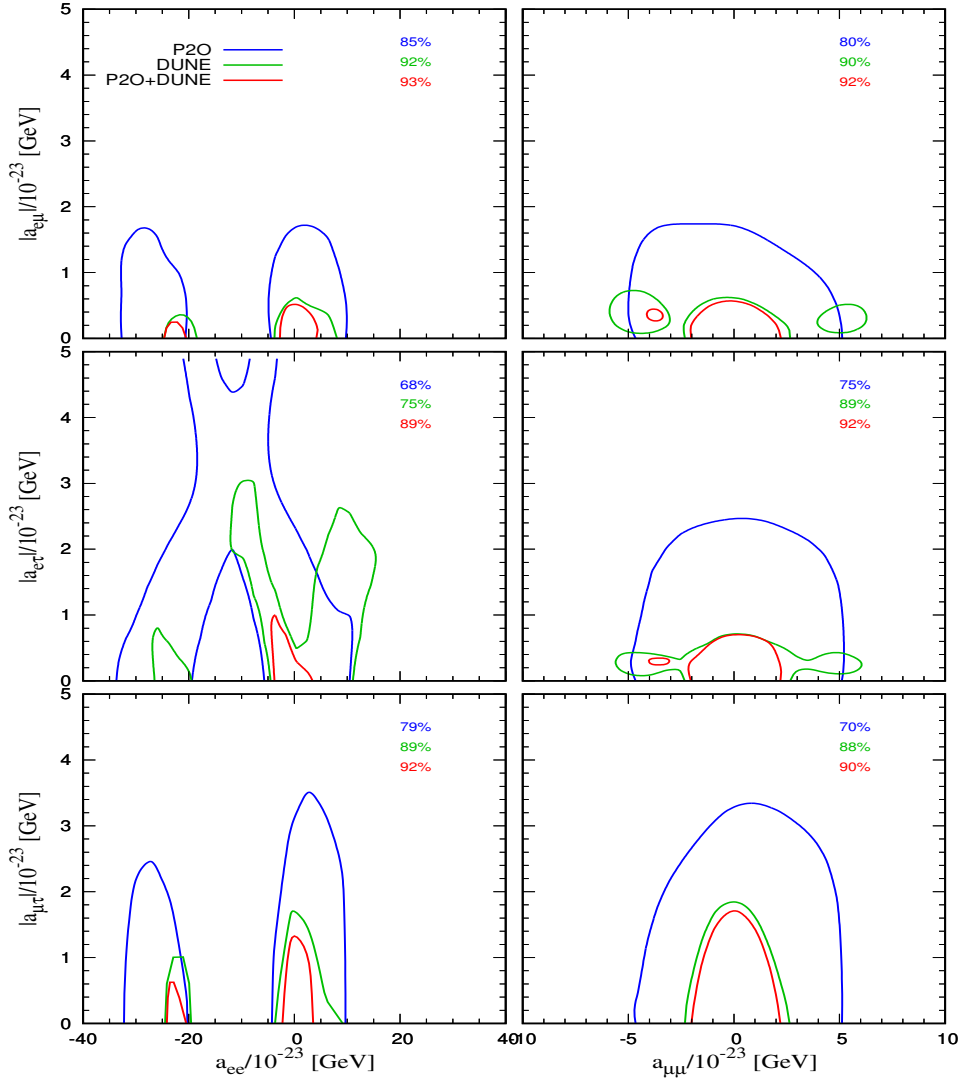


Figure 5. This shows the exclusion regions in the parameter space consisting of one diagonal (along the horizontal axis) and one off-diagonal LIV parameter (vertical axis) for P2O only (blue contours), DUNE only (green contours), and P2O combined with DUNE (red contours). The results are shown at the confidence level (C.L.) of 95%. The triplet of numbers (%) in each panel indicates the area lying (excluded) outside the 95% C.L. contours, expressed as a percentage of the total area of the parameter space considered. The numbers are shown for the three cases, - blue for P2O only, green for DUNE only, and red for the combined case of (P2O + DUNE), and thus they offer a measure of the exclusion capabilities of each experimental configuration for each relevant parameter space.

(P2O + DUNE) hereafter). For completeness we have also shown the analysis with DUNE only case, although that is not the main focus of our work. We refer the interested readers to [41] for a more comprehensive analysis of the capabilities of DUNE to probe LIV pa-

parameter space⁶. For each of these three experimental configurations, namely P2O, DUNE, and (P2O+DUNE), in each panel, we estimate the regions excluded at 95% C.L. contours (*i.e.*, the area outside the contours with blue, green, and red boundaries respectively), and express that as a percentage of the total area of the parameter space is shown. The three numbers thus give us a quantitative measure of the improvement of the combination (P2O + DUNE) over P2O only or DUNE only in excluding the relevant parameter space at 95% C.L.⁷ The improvement is remarkable in almost all cases, covering more than 90% of the parameter space considered. In presence of a_{ee} , we observe the additional/fake degenerate region around $a_{ee} \simeq -22 \times 10^{-23}$ GeV, which arises due to marginalization over the opposite mass hierarchy. Note that the location of this fake solution is approximately opposite in sign to the degeneracies in the corresponding probability heatplots (Figs. 2 and 4: third column, top row), where the additional degeneracies were found around $a_{ee} \simeq 22 \times 10^{-23}$. It can be qualitatively understood as follows. Without considering flux and cross-sections for simplicity, the dominant statistical contribution to the sensitivity in the LIV scenario (*test* scenario) involving the parameter a_{ee} and another parameter, say c , roughly follows the corresponding probability deviation from the *true* standard case (in the similar spirit as discussion in Sec. 3):

$$\Delta\chi^2(a_{ee}, c) \sim \Delta P_{\mu e}(a_{ee}) + \Delta P_{\mu e}(c) + (\text{other terms}), \quad (5.1)$$

where the other terms contain contributions from the $\nu_\mu \rightarrow \nu_\mu$ disappearance channel, antineutrinos, priors and systematics, - which we have neglected in order to have a simple qualitative understanding. Using our previous discussion concerning Eqs. 3.11 and 3.12, we can write,

$$\begin{aligned} \Delta\chi^2(a_{ee}, c) &\sim \Delta P_{\mu e}(a_{ee}) \\ &\sim \underbrace{\left[\frac{\sin [1 - \hat{A}(1 + \hat{a}_{ee})] \Delta}{1 - \hat{A}(1 + \hat{a}_{ee})} - \frac{\sin [1 - \hat{A}] \Delta}{1 - \hat{A}} \right]}_{I_-} \times \underbrace{\left[\frac{\sin [1 - \hat{A}(1 + \hat{a}_{ee})] \Delta}{1 - \hat{A}(1 + \hat{a}_{ee})} + \frac{\sin [1 - \hat{A}] \Delta}{1 - \hat{A}} \right]}_{I_+}. \end{aligned} \quad (5.2)$$

Within the same mass hierarchy for the true and test scenario, the minimum for $\Delta\chi^2(a_{ee}, c)$ is obtained at the true solution $a_{ee} \simeq 0$, making I_- vanish. But while marginalizing over the opposite mass hierarchy in the test scenario, \hat{A} and Δ changes sign in the term $\sin[1 - \hat{A}(1 + \hat{a}_{ee})]\Delta/[1 - \hat{A}(1 + \hat{a}_{ee})]$ containing a_{ee} , and we have,

$$\Delta\chi^2(a_{ee}, c) \sim \underbrace{\left[\frac{\sin [1 + \hat{A}(1 + \hat{a}_{ee})] \Delta}{1 + \hat{A}(1 + \hat{a}_{ee})} + \frac{\sin [1 - \hat{A}] \Delta}{1 - \hat{A}} \right]}_{I_-} \times \underbrace{\left[\frac{\sin [1 + \hat{A}(1 + \hat{a}_{ee})] \Delta}{1 + \hat{A}(1 + \hat{a}_{ee})} - \frac{\sin [1 - \hat{A}] \Delta}{1 - \hat{A}} \right]}_{I_+}. \quad (5.3)$$

⁶The analysis with DUNE-only case in the present work is qualitatively consistent with [41] with some minor differences due to different choices of the set of values of the oscillation parameters, different ranges of marginalization, different minimization techniques *etc.*

⁷Similar estimates were used in reference [78] in order to quantify the improvement of one experimental configuration over another in the context of non-standard neutrino interaction.

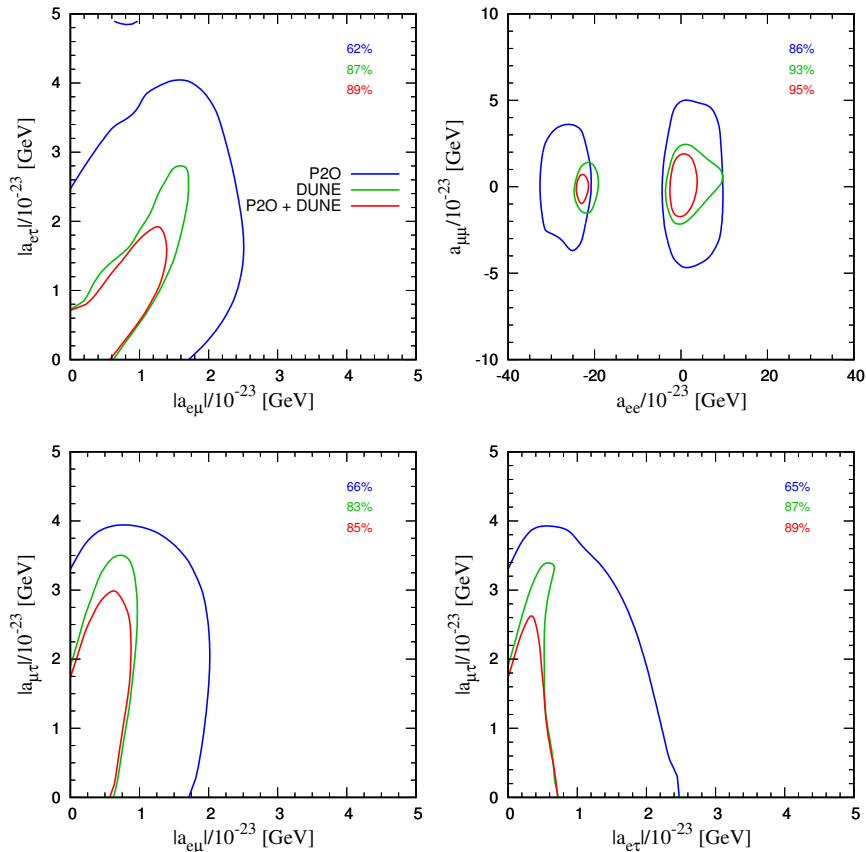


Figure 6. Similar to Fig. 5 but shows the exclusion regions in the parameter spaces with both off-diagonal LIV parameters (top-left, bottom-left and bottom-right panels) and both diagonal LIV parameters (top right panel).

Because of the relative changes of signs, now I_- cannot vanish and the minimum solution is obtained when I_+ goes to zero instead. That is obtained when $\hat{a}_{ee} = -2$ and thus $a_{ee} \simeq -22 \times 10^{-23}$ GeV. Such a degeneracy can also be observed for the DUNE only case (green contours), which is consistent with previous analyses with LIV in case of DUNE [41]. Although a combination with DUNE significantly constrains this additional degeneracy at 95% C.L., it still does not go away completely (we have checked that it still remains at 99% C.L.). For the parameter $a_{\mu\mu}$ we see the contours are roughly symmetric around the true solution $a_{\mu\mu} = 0$. If $a_{\mu\tau}$ is present, a combination with DUNE can probe more than 92% of the entire parameter space considered at a C.L. of 95%. This sensitivity to $|a_{\mu\tau}|$ mainly comes from the $\nu_\mu \rightarrow \nu_\mu$ disappearance channel.

Fig. 6 shows the $\Delta\chi^2$ correlation among the off-diagonal LIV parameters themselves ($|a_{e\mu}|, |a_{e\tau}|, |a_{\mu\tau}|$) and also between the two diagonal parameters a_{ee} and $a_{\mu\mu}$, for P2O, DUNE and (P2O+DUNE). The improvement by the combined analysis is especially prominent for the most impactful parameter space $a_{e\mu} - a_{e\tau}$ (top left panel of Fig. 6). At a C.L. of 95%, (P2O+DUNE) combination can exclude 89% of the parameter ranges considered,

compared to 62% by P2O alone.

6 Degeneracies with the standard oscillation parameters

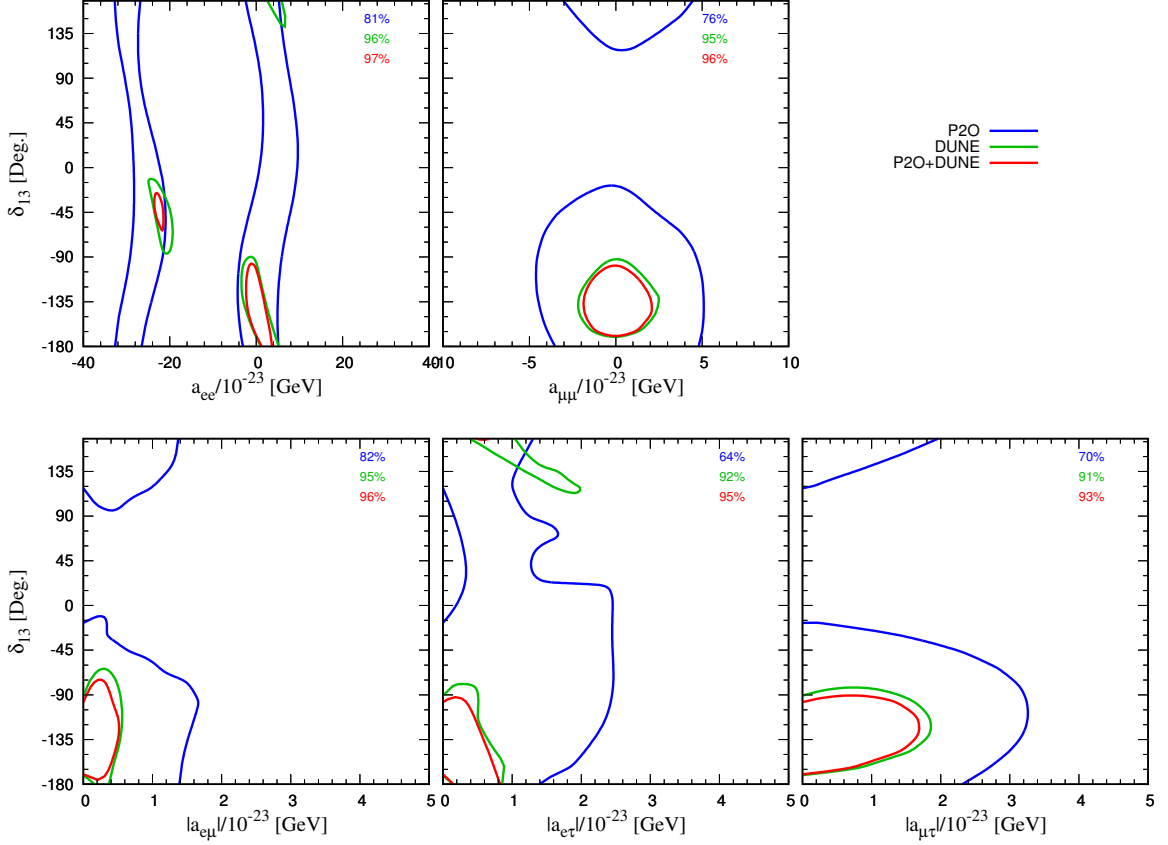


Figure 7. Exclusion regions at 95% C.L., showing the correlations of the LIV parameters with the CP phase δ_{13} for P2O (blue contours), DUNE (green) and P2O+DUNE (red contours). Similar to Fig. 5, the triplet of numbers (%) in each panel indicates the area of parameter space excluded at 95% C.L., expressed as a percentage of the total area of the parameter space considered.

In Fig. 7 (and Fig. 8), we demonstrate how efficiently the projected data from P2O, DUNE and the combined case of (P2O+DUNE) can reconstruct the standard CP phase δ_{13} and mixing angle θ_{23} , in correlation with the LIV parameters present. Here we assume the presence of one LIV parameter at a time and marginalize over the relevant LIV phase, as well as over the standard parameter not shown along the axes (see Table 1 for the ranges and priors.). For instance, for the analysis in the $|a_{e\mu}| - \delta_{13}$ plane, the minimum $\Delta\chi^2$ is obtained after varying Δm_{31}^2 (both magnitude and sign) and θ_{23} with priors of 2.4% and 3.5% respectively and $\varphi_{e\mu}$ without prior in an unrestricted manner. Similarly, for the $|a_{e\mu}| - \theta_{23}$ plane, the marginalization is carried over δ_{13} and $\varphi_{e\mu}$ without priors in an

unrestricted way and over Δm_{31}^2 with a 2.4% prior. At the C.L. of 95%, the presence of any LIV parameter at P2O can give rise to allowed regions covering a large δ_{13} -space (entire δ_{13} -space for a_{ee} and $a_{e\tau}$). But the combination (P2O + DUNE) significantly shrinks the allowed regions to lie around the true solution of $\delta_{13} = -122.4^\circ$. Similar observation holds in Fig. 8 for the parameter space containing θ_{23} also. Concerning the combined analysis of (P2O+DUNE) (*i.e.*, the red contours in Fig. 8), although the maximal mixing ($\theta_{23} = 45^\circ$) got excluded in case of all the LIV parameters, in case of $a_{e\mu}$ and $a_{e\tau}$ (bottom row, first and second columns of Fig. 8) we note that the allowed regions still appear in the opposite (lower) octant. We refer the readers to [43] for a more in-depth discussion regarding the impacts of $a_{e\mu}$ and $a_{e\tau}$ on θ_{23} -octant. It is clear that for P2O alone, the exclusion region in presence of $a_{e\mu}$ is greater than in presence of $a_{e\tau}$ (67% versus 54% of the total parameter space considered, at 95% C.L.). This can be connected to the higher impact of $a_{e\mu}$ in the probability deviation $|\Delta P_{\mu e}|$ in Fig. 4 (top row, first and second column) and related discussions in Sec. 3. a_{ee} generates the additional degeneracy around -22×10^{-23} GeV as usual.

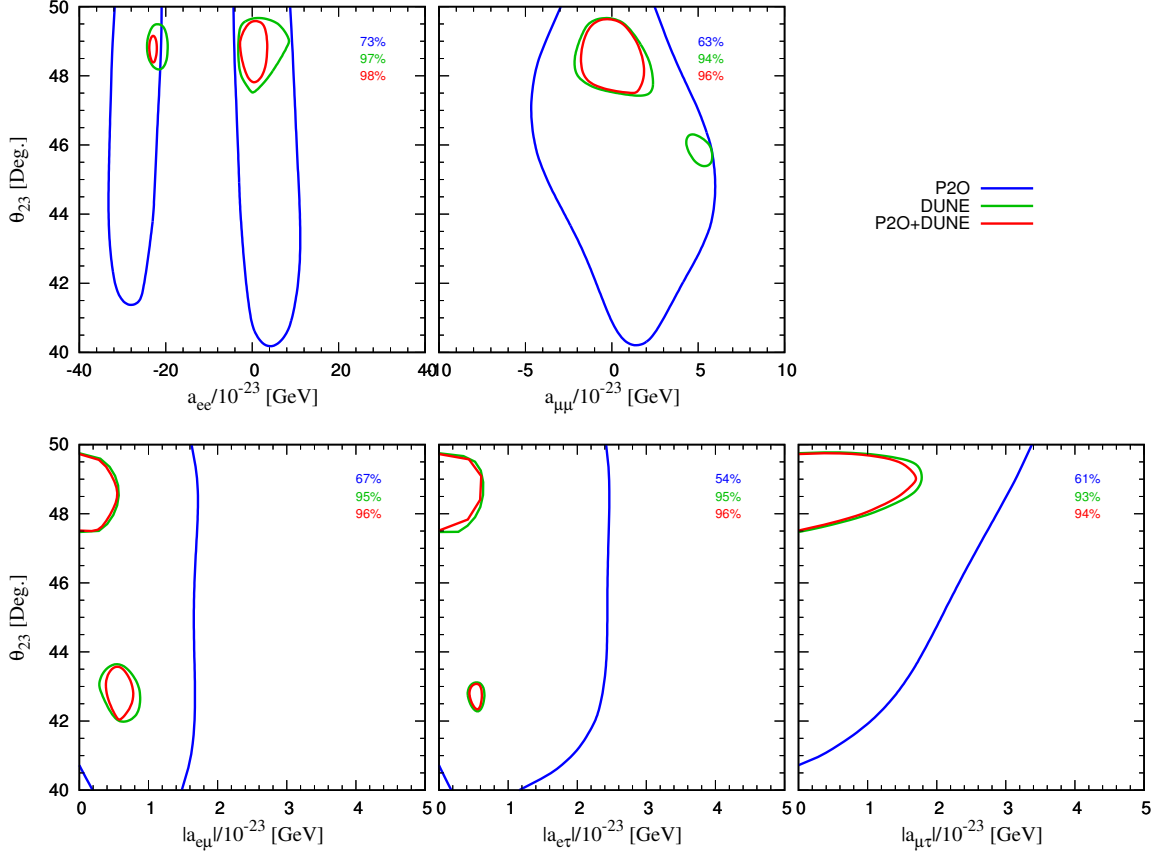


Figure 8. Similar to Fig. 7 but showing the correlation of the LIV parameters with θ_{23} .

7 Bounds on the LIV parameters

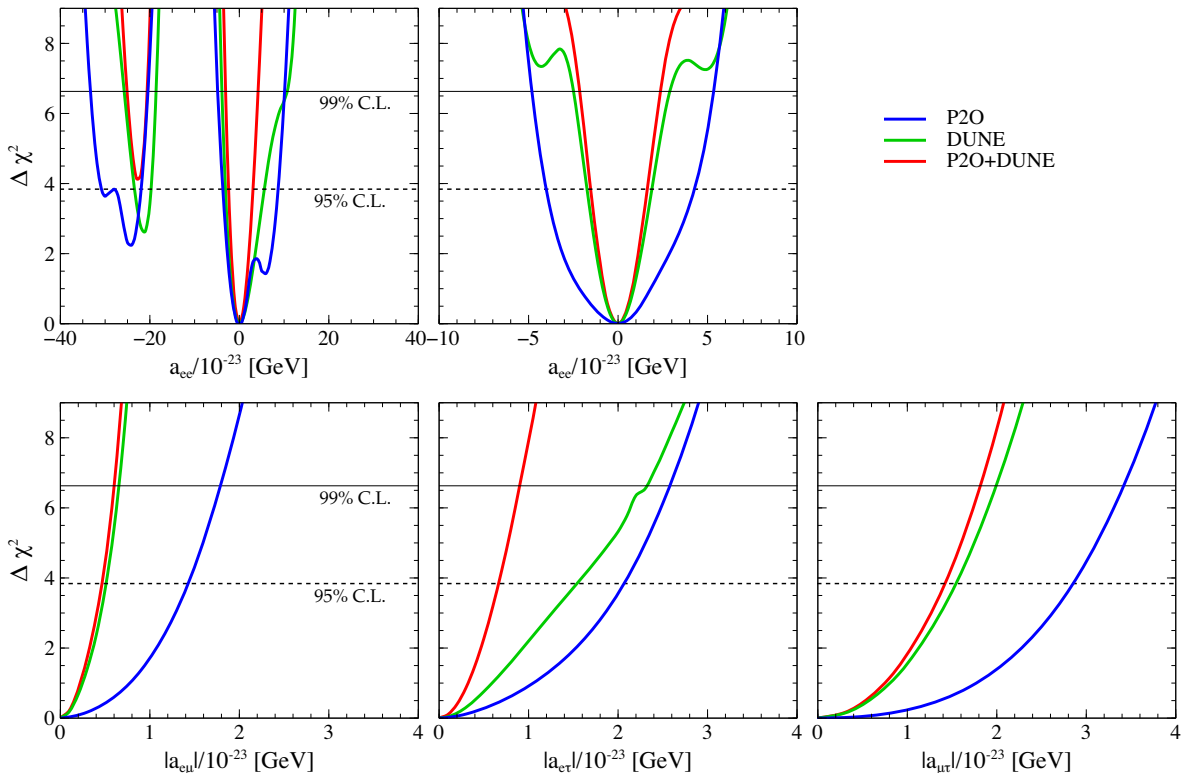


Figure 9. Expected sensitivity of P2O (blue) and the combined (P2O+DUNE) (red) analysis to the LIV parameters. The black dotted (solid) line indicates the 95% (99%) C.L. at 1 degree of freedom. Each panel corresponds to individual LIV parameter.

Parameter	Bounds from DUNE [10^{-23} GeV]	Bounds from P2O [10^{-23} GeV]	Bounds from (P2O+DUNE) [10^{-23} GeV]
a_{ee}	$[-24 < a_{ee} < -20]$ $\cup [-3.2 < a_{ee} < 5.6]$	$[-30.8 < a_{ee} < -21.9]$ $\cup [-3.9 < a_{ee} < 8.6]$	$-2.6 < a_{ee} < 3.3$
$a_{\mu\mu}$	$-1.9 < a_{\mu\mu} < 2.0$	$-4.0 < a_{\mu\mu} < 4.3$	$-1.6 < a_{\mu\mu} < 1.6$
$ a_{e\mu} $	0.6	1.6	0.4
$ a_{e\tau} $	1.3	2.1	0.7
$ a_{\mu\tau} $	1.5	2.9	1.3

Table 3. Bounds on the LIV parameters as obtained from the simulations of LBL data: (DUNE, P2O and (P2O+DUNE) in the 2nd, third, fourth column respectively) at 95% C.L.

Fig. 9 shows the one dimensional projection (after marginalising away all other parameters including the CP phases, θ_{23} , Δm_{31}^2) of $\Delta\chi^2$ as a function of each LIV parameter

individually. The results are illustrated for P2O alone (blue), DUNE alone (green) and for the combined analysis of (P2O + DUNE) (red). The $\Delta\chi^2$ values corresponding to 95% and 99% C.L.s are marked with horizontal black lines. The significant increase in the steepness of the red sensitivity curves is indicative of the crucial impact of the combined analysis in constraining the LIV parameters. For a_{ee} , we note the lifting of the troublesome degeneracy at $a_{ee} \simeq -22 \times 10^{-23}$ GeV by the combined analysis above 95% C.L. This was not possible with the analysis done with DUNE alone (see also [41]) or with P2O alone. Table 3 shows our final result: the constraints obtained on the five LIV parameters at 95% C.L. with the combined (P2O+DUNE) analysis and compares the numbers obtained from only DUNE or only P2O. We note that the constraints on the diagonal parameters can be tightened significantly with the combined analysis. This is especially noticeable for a_{ee} since the fake solution can be ruled out at 95% C.L. as mentioned before. For $|a_{e\mu}|$, $|a_{e\tau}|$ and $|a_{\mu\tau}|$ also the bounds improve moderately. Some comments are in order regarding the bounds on LIV parameters achieved by existing atmospheric neutrino data. Atmospheric neutrino experiments are sensitive to a much wider range of baseline and energy, and hence can obtain strong constraints on LIV parameters. For instance, the SK data have put the following bounds on the LIV parameters at 95% C.L. [33],

$$\begin{aligned} |a_{\mu\mu}| &\lesssim 1.9 \times 10^{-23} \text{ GeV}, \\ \text{Re}(a_{e\mu}), \text{Im}(a_{e\mu}) &\lesssim 1.8 \times 10^{-23} \text{ GeV}; \\ \text{Re}(a_{e\tau}) &\lesssim 4.1 \times 10^{-23} \text{ GeV}; \text{Im}(a_{e\tau}) \lesssim 2.8 \times 10^{-23} \text{ GeV}; \end{aligned}$$

which roughly translate to,

$$\begin{aligned} |a_{e\mu}| &\lesssim 3.2 \times 10^{-23} \text{ GeV}; \\ |a_{e\tau}| &\lesssim 5 \times 10^{-23} \text{ GeV}. \end{aligned}$$

Analysis of high energy astrophysical and atmospheric neutrino at IceCube have put following stronger constraints, at an even higher statistical significance of 99% C.L. [35]:

$$|\text{Re}(a_{\mu\tau})|, |\text{Im}(a_{\mu\tau})| \lesssim 0.29 \times 10^{-23} \text{ GeV} \implies |a_{\mu\tau}| \lesssim 0.41 \times 10^{-23} \text{ GeV}.$$

The next generation IceCube-Gen2 [93] is expected to reach much tighter bounds on LIV parameter space. On the other hand if LBL experiments such as DUNE is also used to collect and analyse atmospheric neutrino data (in addition to beam neutrinos), it becomes sensitive to a much wider range of baseline and energy, and the constraints on LIV parameters can then improve by several orders of magnitude [13]. We would also like to mention that in comparison to LBL data, high energy astrophysical and atmospheric neutrino experiments can become more sensitive to higher order LIV parameters (which are energy-dependent) which we have not considered in the present analysis. As more neutrino data become available in near future, it will be possible to strategically combine LBL and atmospheric neutrino data and search for the presence of LIV with an unprecedented sensitivity reach. However, in the present analysis we have focused on the capability of LBL experiments only to probe the LIV parameters. A full combined analysis of both LBL and atmospheric data (simulated/real data) is beyond the scope of the current work, and we leave it as a future project.

8 Summary and conclusion

In this work we consider the proposed long baseline experiment P2O with a 2595 km baseline from the already existing accelerator complex at Protvino to the far detector situated at the site of KM3NeT/ ORCA with a fiducial mass of approximately 6 Mt. and a peak energy of around 4-5 GeV. Such a long baseline offers very high sensitivity to neutrino mass hierarchy and the massive far detector provides very high statistics even with a relatively moderate 90 kW proton beam. In this work, we have discussed the capability of an LBL experiment to probe fundamental theories of quantum gravity that can potentially manifest itself in the form of Lorentz invariance violation (LIV) around this energy range. We first discuss how the probabilities can deviate from the standard interaction (SI) scenario by different Lorentz invariance violating parameters (which are also CPT-violating) at the P2O baseline. We then analytically derive the approximate changes in the appearance probabilities, $\Delta P_{\mu e}$ ($= P_{\mu e}(\text{SI}+\text{LIV}) - P_{\mu e}(\text{SI})$) that are induced by individual LIV parameters. We illustrate by means of heatplots of $\Delta P_{\mu e}$, how the LIV parameters impact at the baseline of P2O at its peak energy and compare it with DUNE experiment. In presence of $a_{e\mu}$ and $a_{e\tau}$, we find interesting degenerate branches (existing even for larger values of the LIV parameters) at specific values of the standard CP phase δ_{13} . As a function of θ_{23} , we observe that the impact of $a_{e\mu}$ on $\Delta P_{\mu e}$ is slightly higher than that of $a_{e\tau}$. These features were also explained with the help of probability expressions in presence of these two parameters. We also find two degenerate regions at the level of probability for $a_{ee} \simeq 0, 22 \times 10^{-23}$ GeV, whereas for DUNE we find only the trivial one at $a_{ee} = 0$. We explain this by breaking down the corresponding $\Delta P_{\mu e}$ and showing that the relevant *sine*-term oscillates faster for P2O (due to higher peak energy and a slightly higher value of average baseline density), - forcing a second nontrivial solution. We then proceed to estimate $\Delta\chi^2$ sensitivities to LIV parameters for P2O alone and also discuss how significantly the results improve when the simulated data of P2O is combined with that of DUNE. For completeness, we have also compared the results with a similar analysis using the simulated data of only DUNE. The sensitivity analyses were carried out by showing correlations of the LIV parameters ($a_{ee}, a_{\mu\mu}, a_{e\mu}, a_{e\tau}, a_{\mu\tau}$) among themselves and also with the two standard oscillation parameters δ_{13} and θ_{23} . For a_{ee} we discuss in detail analytically how a crucial change in sign due to marginalization over the opposite mass hierarchy produces a *fake* $\Delta\chi^2$ minimum around $a_{ee} \simeq -22 \times 10^{-23}$ GeV. For all the parameter spaces we numerically estimate the area of the regions that are excluded (at 95% C.L.) by P2O (or DUNE) individually and compare it to that by the combined analysis of (P2O + DUNE). The significance quantitative increase in the excluded area for (P2O+DUNE) shows the overwhelming advantage of the combined analysis in all cases. Finally we calculate the one-dimensional $\Delta\chi^2$ projections as a function of all five individual LIV parameters after marginalisation over all other parameters and estimate the 95% C.L. constraints. We find that for the diagonal LIV parameters there is a significant improvement of the constraints estimated with the combined (P2O+DUNE) analysis. Especially noteworthy is the lifting of degeneracy around $a_{ee} \simeq -22 \times 10^{-23}$ GeV, which is not possible with P2O-only or DUNE-only analysis. For the off-diagonal LIV parameters also our estimated bounds improve

moderately.

Acknowledgement

MM acknowledges the support from IBS under the project code IBS-R018-D1. We thank D. Zabarov for providing us with the P2O flux files. NRKC gratefully acknowledges the financial support of the Ministry of Science, Innovation and Universities: State Program of Generation of Knowledge, ref. PGC2018-096663-B-C41 (MCIU / FEDER), Spain. NF is grateful for a visiting position at IBS CTPU where this work was finished. We would also like to thank the anonymous referee for the valuable suggestions.

References

- [1] SUPER-KAMIOKANDE COLLABORATION collaboration, *Evidence for oscillation of atmospheric neutrinos*, *Phys.Rev.Lett.* **81** (1998) 1562 [[hep-ex/9807003](#)].
- [2] SNO collaboration, *Direct evidence for neutrino flavor transformation from neutral current interactions in the Sudbury Neutrino Observatory*, *Phys. Rev. Lett.* **89** (2002) 011301 [[nucl-ex/0204008](#)].
- [3] A. Sakharov, *Violation of CP Invariance, C asymmetry, and baryon asymmetry of the universe*, *Sov. Phys. Usp.* **34** (1991) 392.
- [4] T2K collaboration, *Observation of Electron Neutrino Appearance in a Muon Neutrino Beam*, *Phys. Rev. Lett.* **112** (2014) 061802 [[1311.4750](#)].
- [5] NOVA collaboration, *NOvA: Proposal to Build a 30 Kiloton Off-Axis Detector to Study $\nu_\mu \rightarrow \nu_e$ Oscillations in the NuMI Beamline*, [hep-ex/0503053](#).
- [6] T2K collaboration, *Constraint on the matter–antimatter symmetry-violating phase in neutrino oscillations*, *Nature* **580** (2020) 339 [[1910.03887](#)].
- [7] NOVA collaboration, *First Measurement of Neutrino Oscillation Parameters using Neutrinos and Antineutrinos by NOvA*, *Phys. Rev. Lett.* **123** (2019) 151803 [[1906.04907](#)].
- [8] P. de Salas, D. Forero, S. Gariazzo, P. Martínez-Miravé, O. Mena, C. Ternes et al., *2020 Global reassessment of the neutrino oscillation picture*, [2006.11237](#).
- [9] Valencia-Globalfit. <http://globalfit.astroparticles.es/>, 2020.
- [10] F. Capozzi, E. Di Valentino, E. Lisi, A. Marrone, A. Melchiorri and A. Palazzo, *Global constraints on absolute neutrino masses and their ordering*, *Phys. Rev. D* **95** (2017) 096014 [[2003.08511](#)].
- [11] I. Esteban, M.C. Gonzalez-Garcia, A. Hernandez-Cabezudo, M. Maltoni and T. Schwetz, *Global analysis of three-flavour neutrino oscillations: synergies and tensions in the determination of θ_{23} , δ_{CP} , and the mass ordering*, *JHEP* **01** (2019) 106 [[1811.05487](#)].
- [12] DUNE collaboration, *Long-Baseline Neutrino Facility (LBNF) and Deep Underground Neutrino Experiment (DUNE) Conceptual Design Report Volume 2: The Physics Program for DUNE at LBNF*, [1512.06148](#).
- [13] DUNE collaboration, *Deep Underground Neutrino Experiment (DUNE), Far Detector Technical Design Report, Volume II DUNE Physics*, [2002.03005](#).

- [14] HYPER-KAMIOKANDE PROTO-COLLABORATION collaboration, *Physics potential of a long-baseline neutrino oscillation experiment using a J-PARC neutrino beam and Hyper-Kamiokande*, *PTEP* **2015** (2015) 053C02 [[1502.05199](#)].
- [15] HYPER-KAMIOKANDE collaboration, *Physics potentials with the second Hyper-Kamiokande detector in Korea*, *PTEP* **2018** (2018) 063C01 [[1611.06118](#)].
- [16] ESSNUSB collaboration, *A very intense neutrino super beam experiment for leptonic CP violation discovery based on the European spallation source linac*, *Nucl. Phys. B* **885** (2014) 127 [[1309.7022](#)].
- [17] JUNO collaboration, *Neutrino Physics with JUNO*, *J. Phys. G* **43** (2016) 030401 [[1507.05613](#)].
- [18] A.V. Akhmedov et al., *Letter of Interest for a Neutrino Beam from Protvino to KM3NeT/ORCA*, *Eur. Phys. J. C* **79** (2019) 758 [[1902.06083](#)].
- [19] O.W. Greenberg, *CPT violation implies violation of Lorentz invariance*, *Phys. Rev. Lett.* **89** (2002) 231602 [[hep-ph/0201258](#)].
- [20] V.A. Kostelecky and S. Samuel, *Spontaneous Breaking of Lorentz Symmetry in String Theory*, *Phys. Rev.* **D39** (1989) 683.
- [21] V.A. Kostelecky and S. Samuel, *Phenomenological Gravitational Constraints on Strings and Higher Dimensional Theories*, *Phys. Rev. Lett.* **63** (1989) 224.
- [22] V.A. Kostelecky and R. Potting, *CPT and strings*, *Nucl. Phys.* **B359** (1991) 545.
- [23] V.A. Kostelecky and R. Potting, *CPT, strings, and meson factories*, *Phys. Rev.* **D51** (1995) 3923 [[hep-ph/9501341](#)].
- [24] V.A. Kostelecky and R. Potting, *Expectation values, Lorentz invariance, and CPT in the open bosonic string*, *Phys. Lett.* **B381** (1996) 89 [[hep-th/9605088](#)].
- [25] D. Colladay and V.A. Kostelecky, *CPT violation and the standard model*, *Phys. Rev.* **D55** (1997) 6760 [[hep-ph/9703464](#)].
- [26] D. Colladay and V.A. Kostelecky, *Lorentz violating extension of the standard model*, *Phys. Rev.* **D58** (1998) 116002 [[hep-ph/9809521](#)].
- [27] V.A. Kostelecky, *Gravity, Lorentz violation, and the standard model*, *Phys. Rev. D* **69** (2004) 105009 [[hep-th/0312310](#)].
- [28] LSND collaboration, *Tests of Lorentz violation in anti- $\nu(\mu)$ \rightarrow anti- $\nu(e)$ oscillations*, *Phys. Rev. D* **72** (2005) 076004 [[hep-ex/0506067](#)].
- [29] MINOS collaboration, *Testing Lorentz Invariance and CPT Conservation with NuMI Neutrinos in the MINOS Near Detector*, *Phys. Rev. Lett.* **101** (2008) 151601 [[0806.4945](#)].
- [30] MINOS collaboration, *A Search for Lorentz Invariance and CPT Violation with the MINOS Far Detector*, *Phys. Rev. Lett.* **105** (2010) 151601 [[1007.2791](#)].
- [31] MINIBOONE collaboration, *Test of Lorentz and CPT violation with Short Baseline Neutrino Oscillation Excesses*, *Phys. Lett. B* **718** (2013) 1303 [[1109.3480](#)].
- [32] DOUBLE CHOOZ collaboration, *First Test of Lorentz Violation with a Reactor-based Antineutrino Experiment*, *Phys. Rev. D* **86** (2012) 112009 [[1209.5810](#)].
- [33] SUPER-KAMIOKANDE collaboration, *Test of Lorentz invariance with atmospheric neutrinos*, *Phys. Rev. D* **91** (2015) 052003 [[1410.4267](#)].

- [34] T2K collaboration, *Search for Lorentz and CPT violation using sidereal time dependence of neutrino flavor transitions over a short baseline*, *Phys. Rev. D* **95** (2017) 111101 [[1703.01361](#)].
- [35] ICECUBE collaboration, *Neutrino Interferometry for High-Precision Tests of Lorentz Symmetry with IceCube*, *Nature Phys.* **14** (2018) 961 [[1709.03434](#)].
- [36] A. Dighe and S. Ray, *CPT violation in long baseline neutrino experiments: A Three flavor analysis*, *Phys.Rev.* **D78** (2008) 036002 [[0802.0121](#)].
- [37] G. Barenboim and J.D. Lykken, *MINOS and CPT-violating neutrinos*, *Phys. Rev.* **D80** (2009) 113008 [[0908.2993](#)].
- [38] B. Rebel and S. Mufson, *The Search for Neutrino-Antineutrino Mixing Resulting from Lorentz Invariance Violation using neutrino interactions in MINOS*, *Astropart. Phys.* **48** (2013) 78 [[1301.4684](#)].
- [39] A. de Gouvêa and K.J. Kelly, *Neutrino vs. Antineutrino Oscillation Parameters at DUNE and Hyper-Kamiokande*, *Phys. Rev. D* **96** (2017) 095018 [[1709.06090](#)].
- [40] G. Barenboim, C.A. Ternes and M. Tórtola, *Neutrinos, DUNE and the world best bound on CPT violation*, [1712.01714](#).
- [41] G. Barenboim, M. Masud, C.A. Ternes and M. Tórtola, *Exploring the intrinsic Lorentz-violating parameters at DUNE*, *Phys. Lett. B* **788** (2019) 308 [[1805.11094](#)].
- [42] R. Majhi, S. Chembra and R. Mohanta, *Exploring the effect of Lorentz invariance violation with the currently running long-baseline experiments*, *Eur. Phys. J. C* **80** (2020) 364 [[1907.09145](#)].
- [43] S. Kumar Agarwalla and M. Masud, *Can Lorentz invariance violation affect the sensitivity of deep underground neutrino experiment?*, *Eur. Phys. J. C* **80** (2020) 716 [[1912.13306](#)].
- [44] U. Rahaman, *Looking for Lorentz invariance violation (LIV) in the latest long baseline accelerator neutrino oscillation data*, *Eur. Phys. J. C* **81** (2021) 792 [[2103.04576](#)].
- [45] C. Giunti and M. Laveder, *Hint of CPT Violation in Short-Baseline Electron Neutrino Disappearance*, *Phys. Rev.* **D82** (2010) 113009 [[1008.4750](#)].
- [46] A. Datta, R. Gandhi, P. Mehta and S.U. Sankar, *Atmospheric neutrinos as a probe of CPT and Lorentz violation*, *Phys. Lett.* **B597** (2004) 356 [[hep-ph/0312027](#)].
- [47] A. Chatterjee, R. Gandhi and J. Singh, *Probing Lorentz and CPT Violation in a Magnetized Iron Detector using Atmospheric Neutrinos*, *JHEP* **1406** (2014) 045 [[1402.6265](#)].
- [48] B. Singh Koranga and P. Khurana, *CPT Violation in Atmospheric Neutrino Oscillation: A Two Flavour Matter Effects*, *Int. J. Theor. Phys.* **53** (2014) 3737.
- [49] S. Sahoo, A. Kumar and S.K. Agarwalla, *Probing Lorentz Invariance Violation with atmospheric neutrinos at INO-ICAL*, *JHEP* **03** (2022) 050 [[2110.13207](#)].
- [50] J.S. Diaz and T. Schwetz, *Limits on CPT violation from solar neutrinos*, *Phys. Rev.* **D93** (2016) 093004 [[1603.04468](#)].
- [51] D. Hooper, D. Morgan and E. Winstanley, *Lorentz and CPT invariance violation in high-energy neutrinos*, *Phys. Rev.* **D72** (2005) 065009 [[hep-ph/0506091](#)].
- [52] G. Tomar, S. Mohanty and S. Pakvasa, *Lorentz Invariance Violation and IceCube Neutrino Events*, *JHEP* **11** (2015) 022 [[1507.03193](#)].

- [53] J. Liao and D. Marfatia, *IceCube's astrophysical neutrino energy spectrum from CPT violation*, *Phys. Rev.* **D97** (2018) 041302 [[1711.09266](#)].
- [54] H.-X. Lin, P. Pasquini, J. Tang and S. Vihonen, *Nonminimal Lorentz invariance violation in light of the muon anomalous magnetic moment and long-baseline neutrino oscillation data*, *Phys. Rev. D* **105** (2022) 096029 [[2111.14336](#)].
- [55] V.A. Kostelecky and N. Russell, *Data Tables for Lorentz and CPT Violation*, [0801.0287](#).
- [56] D. Zaborov, “Scientific Potential of a neutrino beam from Protvino to ORCA (P2O).” talk at Neutrino GDR Meeting, Paris, November 2017.
”<https://indico.in2p3.fr/event/16553/contributions/57491/attachments/45237/56246/P20-zaborov-GDR-neutrino-Nov2017.pdf>”, 2017.
- [57] KM3NET collaboration, *Letter of intent for KM3NeT 2.0*, *J. Phys. G* **43** (2016) 084001 [[1601.07459](#)].
- [58] KM3NET collaboration, *The KM3NeT Neutrino Telescope and the potential of a neutrino beam from Russia to the Mediterranean Sea*, in *18th Lomonosov Conference on Elementary Particle Physics*, pp. 53–60, 2019, DOI [[1803.08017](#)].
- [59] P. Coloma and P. Huber, *Impact of nuclear effects on the extraction of neutrino oscillation parameters*, *Phys. Rev. Lett.* **111** (2013) 221802 [[1307.1243](#)].
- [60] U. Mosel, O. Lalakulich and K. Gallmeister, *Energy reconstruction in the Long-Baseline Neutrino Experiment*, *Phys. Rev. Lett.* **112** (2014) 151802 [[1311.7288](#)].
- [61] L. Alvarez-Ruso, Y. Hayato and J. Nieves, *Progress and open questions in the physics of neutrino cross sections at intermediate energies*, *New J. Phys.* **16** (2014) 075015 [[1403.2673](#)].
- [62] O. Benhar, P. Huber, C. Mariani and D. Meloni, *Neutrino–nucleus interactions and the determination of oscillation parameters*, *Phys. Rept.* **700** (2017) 1 [[1501.06448](#)].
- [63] NuSTEC collaboration, *NuSTEC White Paper: Status and challenges of neutrino–nucleus scattering*, *Prog. Part. Nucl. Phys.* **100** (2018) 1 [[1706.03621](#)].
- [64] S. Nagu, J. Singh and J. Singh, *Nuclear Effects and CP Sensitivity at DUNE*, *Adv. High Energy Phys.* **2020** (2020) 5472713 [[1906.02190](#)].
- [65] D.K. Singha, M. Ghosh, R. Majhi and R. Mohanta, *Optimal configuration of Protvino to ORCA experiment for hierarchy and non-standard interactions*, *JHEP* **05** (2022) 117 [[2112.04876](#)].
- [66] S. Choubey, M. Ghosh and D. Pramanik, *Sensitivity study of Protvino to ORCA (P2O) experiment: effect of antineutrino run, background and systematics*, *Eur. Phys. J. C* **79** (2019) 603 [[1812.02608](#)].
- [67] M. Perrin-Terrin, *Neutrino tagging: a new tool for accelerator based neutrino experiments*, *Eur. Phys. J. C* **82** (2022) 465 [[2112.12848](#)].
- [68] D. Kaur, N.R.K. Chowdhury and U. Rahaman, *Effect of non-unitary mixing on the mass hierarchy and CP violation determination at the Protvino to Orca experiment*, [2110.02917](#).
- [69] V.A. Kostelecky and R. Lehnert, *Stability, causality, and Lorentz and CPT violation*, *Phys. Rev. D* **63** (2001) 065008 [[hep-th/0012060](#)].
- [70] V.A. Kostelecky and M. Mewes, *Lorentz and CPT violation in neutrinos*, *Phys. Rev.* **D69** (2004) 016005 [[hep-ph/0309025](#)].

- [71] J.S. Diaz, V.A. Kostelecky and M. Mewes, *Perturbative Lorentz and CPT violation for neutrino and antineutrino oscillations*, *Phys. Rev. D* **80** (2009) 076007 [[0908.1401](#)].
- [72] A. Kostelecky and M. Mewes, *Neutrinos with Lorentz-violating operators of arbitrary dimension*, *Phys. Rev.* **D85** (2012) 096005 [[1112.6395](#)].
- [73] V.A. Kostelecky and M. Mewes, *Signals for Lorentz violation in electrodynamics*, *Phys. Rev. D* **66** (2002) 056005 [[hep-ph/0205211](#)].
- [74] J.S. Diaz and A. Kostelecky, *Lorentz- and CPT-violating models for neutrino oscillations*, *Phys. Rev. D* **85** (2012) 016013 [[1108.1799](#)].
- [75] J.S. Diaz, *Correspondence between nonstandard interactions and CPT violation in neutrino oscillations*, [1506.01936](#).
- [76] T. Kikuchi, H. Minakata and S. Uchinami, *Perturbation Theory of Neutrino Oscillation with Nonstandard Neutrino Interactions*, *JHEP* **0903** (2009) 114 [[0809.3312](#)].
- [77] S.K. Agarwalla, S.S. Chatterjee and A. Palazzo, *Degeneracy between θ_{23} octant and neutrino non-standard interactions at DUNE*, *Phys. Lett. B* **762** (2016) 64 [[1607.01745](#)].
- [78] M. Masud, S. Roy and P. Mehta, *Correlations and degeneracies among the NSI parameters with tunable beams at DUNE*, *Phys. Rev. D* **99** (2019) 115032 [[1812.10290](#)].
- [79] P. Huber, M. Lindner and W. Winter, *Simulation of long-baseline neutrino oscillation experiments with GLoBES (General Long Baseline Experiment Simulator)*, *Comput. Phys. Commun.* **167** (2005) 195 [[hep-ph/0407333](#)].
- [80] P. Huber, J. Kopp, M. Lindner, M. Rolinec and W. Winter, *New features in the simulation of neutrino oscillation experiments with GLoBES 3.0: General Long Baseline Experiment Simulator*, *Comput. Phys. Commun.* **177** (2007) 432 [[hep-ph/0701187](#)].
- [81] J. Kopp, *Efficient numerical diagonalization of hermitian 3 x 3 matrices*, *Int. J. Mod. Phys. C* **19** (2008) 523 [[physics/0610206](#)].
- [82] J. Kopp, M. Lindner, T. Ota and J. Sato, *Non-standard neutrino interactions in reactor and superbeam experiments*, *Phys. Rev.* **D77** (2008) 013007 [[0708.0152](#)].
- [83] DUNE collaboration, *Experiment Simulation Configurations Used in DUNE CDR*, [1606.09550](#).
- [84] KM3NET collaboration, *Letter of Intent for KM3NeT2.0*, [1601.07459](#).
- [85] KM3NET collaboration, *The KM3NeT infrastructure: status and first results*, in *21st International Symposium on Very High Energy Cosmic Ray Interactions*, 8, 2022 [[2208.07370](#)].
- [86] P2O collaboration, J. Brunner, “Neutrino Beam from Protvino to KM3NeT/ORCA.” contribution at European Strategy for Particle Physics (2018-2020). ”https://indico.cern.ch/event/765096/contributions/3295791/attachments/1785302/2906340/Addendum_P20.pdf”, 2018.
- [87] P2O collaboration, J. Brunner, “P2O Status and current results.” talk at P2O longbaseline Project, January, 2021. ”https://indico.cern.ch/event/997165/contributions/4189633/attachments/2175114/3672699/Intro_210121.pdf”, 2021.
- [88] P. Huber, M. Lindner and W. Winter, *Superbeams versus neutrino factories*, *Nucl. Phys.* **B645** (2002) 3 [[hep-ph/0204352](#)].

- [89] G.L. Fogli, E. Lisi, A. Marrone, D. Montanino and A. Palazzo, *Getting the most from the statistical analysis of solar neutrino oscillations*, *Phys. Rev.* **D66** (2002) 053010 [[hep-ph/0206162](#)].
- [90] M. Gonzalez-Garcia and M. Maltoni, *Atmospheric neutrino oscillations and new physics*, *Phys.Rev.* **D70** (2004) 033010 [[hep-ph/0404085](#)].
- [91] R. Gandhi, P. Ghoshal, S. Goswami, P. Mehta, S.U. Sankar and S. Shalgar, *Mass Hierarchy Determination via future Atmospheric Neutrino Detectors*, *Phys. Rev.* **D76** (2007) 073012 [[0707.1723](#)].
- [92] X. Qian, A. Tan, W. Wang, J.J. Ling, R.D. McKeown and C. Zhang, *Statistical Evaluation of Experimental Determinations of Neutrino Mass Hierarchy*, *Phys. Rev.* **D86** (2012) 113011 [[1210.3651](#)].
- [93] ICECUBE collaboration, *IceCube-Gen2: A Vision for the Future of Neutrino Astronomy in Antarctica*, [1412.5106](#).